Atmos. Chem. Phys. Discuss., 9, 25737–25797, 2009
www.atmos-chem-phys-discuss.net/9/25737/2009/

Atmospheric
Chemistry
and Physics
Discussions

Measurements of iodine monoxide at a semi polluted coastal location

K. L. Furneaux[1,†], L. K. Whalley[1,5], D. E. Heard[1], H. M. Atkinson[1,*], W. J. Bloss[1,], M. J. Flynn[2], M. W. Gallagher[2], T. Ingham[1,5], L. Kramer[3,***], J. D. Lee[4,6], R. Leigh[3], G. B. McFiggans[2], A. S. Mahajan[1], P. S. Monks[3], H. Oetjen[1], J. M. C. Plane[1], and J. D. Whitehead[2]**

[1]School of Chemistry, University of Leeds, Woodhouse Lane, Leeds, LS2 9JT, UK
[2]Centre for Atmospheric Sciences, School of Earth, Atmospheric Environmental Sciences, University of Manchester, Manchester, M13 9PL, UK
[3]Earth Observation Science, Space Research Centre, Department of Physics and Astronomy, University of Leicester, University Road, Leicester, LE1 7RH, UK
[4]Department of Chemistry, University of York, Heslington, York, YO10 5DD, UK
[5]National Centre for Atmospheric Sciences, University of Leeds, Leeds, LS2 9JT, UK
[6]National Centre for Atmospheric Sciences, University of York, Heslington, York, YO10 5DD, UK
[*]now at: British Antarctic Survey,Madingley Road, Cambridge, CB3 0ET, UK

Title Page
Abstract | Introduction
Conclusions | References
Tables | Figures
◀| |▶
◀ ▶
Back | Close
Full Screen / Esc
Printer-friendly Version
Interactive Discussion

[**] now at: School of Geography, Earth Environmental Sciences, University of Birmingham, Edgbaston, Birmingham, B15 2TT, UK
[***] now at: Departments of Geological and Mining Engineering and Sciences and Civil & Environmental Engineering, Michigan, Technological University, 1400 Townsend Dr., Houghton, MI 49931, USA
[†] sadly passed away 28 July 2009

Received: 27 October 2009 – Accepted: 16 November 2009 – Published: 1 December 2009

Correspondence to: D. E. Heard (d.e.heard@leeds.ac.uk)

Published by Copernicus Publications on behalf of the European Geosciences Union.

Abstract

Point source measurements of IO by laser induced fluorescence spectroscopy were made at a semi-polluted coastal location during the Reactive Halogens in the Marine Boundary Layer campaign in September 2006. The site, on the NW French coast, was characterised by extensive intertidal macroalgae beds which were exposed at low tide. The closest known iodine active macroalgae beds were at least 300 m from the measurement point. From 20 days of measurements, IO was observed above the instrument limit of detection on 14 days, of which a clear diurnal profile was observed on 11 days. The maximum IO mixing ratio was 30.0 pptv (10 s integration period) during the day, amongst the highest concentrations ever observed in the atmosphere, and 1–2 pptv during the night. IO concentrations were strongly dependent on tidal height, the intensity of solar irradiation and meteorological conditions. An intercomparison of IO measurements made using point source and spatially averaged DOAS instruments confirms the presence of hot-spots of IO caused by an inhomogeneous distribution of macroalgae. The co-incident, point source measurement of IO and ultra fine particles (2.5 nm≥d≥10 nm) displayed a strong correlation, providing evidence that IO is involved in the production pathway of ultra fine particles at coastal locations. Finally, a modelling study shows that high IO concentrations which are likely to be produced in a macrolagae rich environment can significantly perturb the concentrations of OH and HO_2 radicals. The effect of IO on HO_x is reduced as NO_x concentrations increase.

1 Introduction

The IO radical can impact several important atmospheric chemistry processes through its reaction pathways and cycles. These include partitioning of HO_x and NO_x (McFiggans et al., 2000, Platt and Hönninger, 2003, Bloss et al., 2005), ozone depletion (Davis et al., 1996, Read et al., 2008), formation and growth of new particles (Hoffmann et al., 2001, O'Dowd et al., 2002, McFiggans et al., 2004) and liberation of halogens from sea salt (Vogt et al., 1996, McFiggans et al., 2002).

Iodine species are present at coastal and open ocean regions due to the release of I_2 and halocarbons from macroalgae and microalgae. The daytime IO source is photolysis of these molecules to yield iodine atoms, which react with ozone to produce IO (Reactions R1 and R2). The subsequent photolysis of IO results in a steady-state between IO and I. If IO reacts with itself, BrO, HO_2 or NO_2, O_3 destruction can occur (e.g. Mahajan et al., 2009, for the field site presented in this paper). The night-time source of IO is proposed to be the reaction of I_2 with NO_3 (Reaction R3) followed by the subsequent reaction of I with O_3 (Chambers et al., 1992). Recent modelling calculations confirm that this is the likely pathway to night-time IO (Kaltsoyannis and Plane, 2008).

$$I_2 + h\nu \rightarrow 2I \tag{R1}$$

$$I + O_3 \rightarrow IO + O_2 \tag{R2}$$

$$I_2 + NO_3 \rightarrow I + INO_3 \tag{R3}$$

Halogen activity has been observed at many mid-latitude coastal locations including Mace Head (Ireland) (Alicke et al., 1999, Allan et al., 2000, Saiz-Lopez and Plane, 2004), Brittany (NW France), the North Sea coast (Germany) (Peters et al., 2005), Appledore Island (USA) (Stutz et al., 2007), Tenerife (Canary Islands) (Allan et al., 2000) and Cape Grim (Australia) (Allan et al., 2000, Cainey et al., 2007). Mace Head provides the only positive observation of night-time IO to date (Saiz-Lopez and Plane, 2004). These sites provide a mixture of I atom sources dominated by either I_2 or iodocarbons. The measurements presented in this paper were made at Roscoff, a coastal site on the NW coast of France, as part of the Reactive Halogens in the Marine Boundary Layer (RHaMBLe) programme. RHaMBLe aimed to quantify the impacts of marine halogen emissions on atmospheric composition. An overview of the RHaMBLe programme, including its motivations and objectives, is provided by McFiggans et al. (2009).

The RHaMBLe-Roscoff campaign was unique because it provided a comparison of a variety of point source and spatially averaged detection methods in a semi-polluted environment. The majority of IO observations have taken place in low NO_x environments (West Ireland, Tenerife, NW France, Cape Grim, Antarctica and the Arctic) with the exception of the daytime detection of IO at Appledore Island, Gulf of Maine, when 1–4 pptv of IO was detected in the presence of 5–10 ppbv of NO_2 (Stutz et al., 2007). This paper presents comparisons of IO measurements with different spatial footprints and simultaneous point source IO and particle measurements. Previously, the majority of IO measurements have used long-path differential optical absorption spectroscopy (LP-DOAS), which provides an average IO concentration over several kilometers of the light path. The use of laser induced fluorescence spectroscopy (LIF) provides a point source measurement at time resolutions as short as one second. Combined with measurements from instruments such as LP-DOAS, a greater understanding of the spatial distribution of IO is possible. As chemistry models are normally constrained by point source measurements (e.g. O_3, NO, NO_2 and photolysis frequencies), LIF IO measurements can provide a more appropriate model constraint. It is often necessary to interpret field data and the associated theoretical implications through the use of hot-spot emissions of I_2 due to concentrated emissions from macroalgae beds, rather than homogeneous emissions over a wider area (Pechtl et al., 2006, Kanaya et al., 2002, Sommariva et al., 2006, Saiz-Lopez et al., 2006). The field observations from Roscoff aim to address and validate this approach.

The formation of new particles in coastal environments via a mechanism involving iodine oxides has not been categorically proven, despite laboratory efforts and a number field studies (Cox et al., 1999, Hoffmann et al., 2001, O'Dowd et al., 2002, Makela et al., 2002, Jimenez et al., 2003, McFiggans et al., 2004, Burkholder et al., 2004, Palmer et al., 2005, Sellegri et al., 2005, Pirjola et al., 2005, Saiz-Lopez et al., 2006). Laboratory studies and theoretical calculations show that I_2O_3 and I_2O_5 are the most likely iodine oxide species to form new particles at ambient conditions, which appear to be composed of I_2O_5 (Saunders and Plane, 2005, Kaltsoyannis and Plane, 2008), although uptake of HIO_3 from the gas phase onto pre-existing aerosols has also been proposed (Pechtl et al., 2007). In open ocean regions new particle formation occurs via sulphur containing species but in coastal regions an additional nucleating component has been postulated to be required (O'Dowd et al., 1999, Kulmala et al., 2000). The following reaction scheme is suggested to lead to new particle formation (Reactions R4–R9; Hoffmann et al., 2001, Jimenez et al., 2003, Burkholder et al., 2004, Saunders and Plane, 2005, Kaltsoyannis and Plane, 2008).

$$IO+IO \rightarrow I_2O_2 \tag{R4}$$

$$I_2O_2+O_3 \rightarrow I_2O_3+O_2 \tag{R5}$$

$$IO+OIO \rightarrow I_2O_3 \tag{R6}$$

$$I_2O_3+O_3 \rightarrow I_2O_4+O_2 \tag{R7}$$

$$OIO+OIO \rightarrow I_2O_4 \tag{R8}$$

$$I_2O_4+O_3 \rightarrow I_2O_5+O_2 \tag{R9}$$

Field observations of iodine species within aerosols and precipitation, however, have found low levels of iodate compared to iodide and soluble organically bound iodine, which may be inconsistent with this production pathway and introduces some uncertainty (Gilfedder et al., 2008). Additionally, experimental work has provided evidence for the photolysis of OIO to form exclusively I+O_2 (Gomez Martin et al., 2009), which could compromise the proposed reaction pathway. Most recently, Mahajan et al. (2009) have suggested that particle formation at coastal sites may only occur via a sub-section of the above Reactions (R4, R6 and R8) with the I_2O_4 formed acting as a nucleant and the I_2O_3 condensing on to any existing I_2O_4 clusters. Despite uncertainties associated with the formation of new particles, coordinated observations provide strong evidence that new particle formation in coastal locations occurs via a mechanism involving iodine oxides.

Field measurements at Mace Head during the NAMBLEX campaign were the first coordinated measurements of in situ I_2 and ultra-fine particles (diameter 10 nm) (Heard et al., 2006). In combination with a modelling study, these measurements provided further evidence that I_2 is a necessary precursor to particle events (Saiz-Lopez et al., 2006). The measurements presented here from Roscoff provide the coordinated measurements of in situ IO and ultra-fine particles, providing further evidence of the role of IO in particle formation pathways.

The Leeds LIF IO instrument was deployed for the first time during the RHaMBLe-Roscoff campaign, providing the first measurements of ambient IO by LIF (Whalley et al., 2007). A range of other instruments were deployed during this campaign, providing gas and aerosol measurements, as described by McFiggans et al. (2009). This paper presents measurements of IO from the RHaMBLe-Roscoff field campaign. Section 2 describes the field site and instrumentation. Section 3 presents point source measurements of IO, including a discussion of the influences on IO chemistry at the field site, a comparison of IO measurements by point source and spatially averaged instruments, followed by a discussion of the link between IO and new particle formation. Section 4 discusses the impact of IO on daytime OH and HO_2.

2 Methods and instrumentation

2.1 The field site at Roscoff

Field observations were made at Roscoff, a small town on the NW Atlantic coast of France (48.726° N, 3.988° W) during September 2006 (McFiggans et al., 2009). The sea-beds surrounding Roscoff have a dense coverage of intertidal macroalgae, including inhomogeneously distributed beds of *Laminaria* and *Ascophyllum* which are exposed at low tide (Fig. 1). The macroalgae speciation at Roscoff indicates that the closest macroalgae beds that strongly emit iodine compounds were 300 m from the LIF instrument. Further details on the macroalgae distribution at Roscoff can be found in Leigh et al. (2009). During the campaign the tidal range was near its annual maximum (the maximum tidal range during the campaign was 9.25 m).

The measurement site was located directly on the Roscoff sea front (Fig. 2). During the campaign air masses were predominantly north Atlantic in origin. NO_x levels ($NO+NO_2$) were high throughout the campaign (approximately 1–5 ppbv), due to the proximity of the measurement site to the town (the site was adjacent to a minor road). There was one day of clean air with NO_x less than 1 ppbv.

2.2 Instrumentation

This paper presents measurements of IO by LIF, details of other measurements during the campaign can be found in McFiggans et al. (2009) and references therein. A full description of the instrument can be found in Whalley et al. (2007). In brief, ambient air is sampled through a conical nozzle with a pinhole diameter of 0.8 mm (flow rate =5 slm) into a LIF cell held at 150 Torr. The (2,0) band of the IO $A^2\Pi_{3/2}\leftarrow X^2\Pi_{3/2}$ electronic transition at approximately 445 nm (generated by an all solid-state Nd:YAG pumped Ti:Sapphire laser) is used to electronically excite the IO radical, with off-resonance fluorescence detection of the (2,5) band at 521 nm. Laser scattered light is filtered out using a 520.3 nm centred bandpass filter. Fluorescence is collected using a channeltron photomultiplier (CPM), with the signal recorded by a computer controlled gated photon counter. The instrument collection cycle was either 50 s or 150 s on-resonance collection, followed by a temporally identical off-line collection period to measure the background signal. Data were collected at 10 s intervals and scattered solar light was subtracted for each data point. The laser wavelength was determined by a wavemeter, with the off-line position 0.004–0.006 nm below the IO excitation wavelength (online wavelength position 444.887 nm and offline position typically 444.882 nm).

Daily calibrations were performed throughout the campaign to determine the sensitivity of the IO LIF instrument. Photolysis at 184.9 nm of $N_2O/CF_3I/N_2$ mixtures was used to generate IO between 10 to 150 pptv. Ozone actinometry was used to determine the lamp flux, allowing calculation of the concentrations of IO produced. Potential interferences due to NO_2 fluorescence or laser generated IO were ruled out by laboratory experiments (Whalley et al., 2007).

The instrument is capable of providing a high temporal resolution. Throughout the campaign, the minimum online collection period was 10 s. The sensitivity of the instrument decreased gradually throughout the campaign due to degradation of the CPM response, which resulted in the limit of detection of the instrument increasing by a factor of ten over the campaign. When the instrument was performing at its best the limit of detection was 0.4 pptv over a 150 s integration period (defined by Whalley et al., 2007).

The LIF IO instrument was located in a shipping container adjacent to the seawall and a small jetty at the edge of the town (Fig. 2). The LIF cell was located on the roof of the shipping container with the inlet pinhole at a height of 3.5 m above ground level. At high tide the LIF cell was approximately 3.5 m horizontally displaced from the water.

Measurements of NO and NO_2 were made simultaneously from an inlet located on the CMAX-DOAS mast on the Leicester container at a height of 3.5 m using two chemiluminescence NO detectors (Ecophysics CLD780TR); NO_2 was detected as NO after photolytic conversion.

2.3 Model description

A photochemical box model has been developed to investigate halogen chemistry at Roscoff using the Master Chemical Mechanism version 3.1 (MCM) (Jenkin et al., 1997, 2003, Saunders et al., 2003). The model contains reaction schemes for C1–C4 hydrocarbons which are subject to oxidation by OH, O_3 and NO_3 (216 hydrocarbon species and approximately 580 reactions), and gas phase iodine and bromine chemistry (24 iodine and bromine species and approximately 100 iodine and bromine reactions). The differential equation solver *FACSIMILE for Windows* (MCPA software) was used to process the model. Photolysis rates of the halogen species were calculated from spectral radiometer measurements of the wavelength resolved actinic flux. The rate of heterogeneous loss due to uptake of gaseous species onto aerosol was calculated for each species, according to the aerosol volumetric surface area, reactive uptake coefficient and mean molecular speed using Eq. 1 (Ravishankara, 1997), and was treated as a permanent, irreversible loss. A constant aerosol volumetric surface area of $4\times10^{-6}\,\mathrm{cm}^2\,\mathrm{cm}^{-3}$ was used, representative of typical aerosol values measured during the campaign (Whitehead et al., 2009). Treating heterogeneous loss as a permanent loss for halogen species neglects aqueous processes which can result in the re-release of gaseous halogen species (Pechtl et al., 2007, Vogt et al., 1999, McFiggans et al., 2000); the recycling of IO presented here may therefore represent a lower limit, but allows the magnitude of gas-phase recycling to be determined explicitly. A list of the halogen chemistry reaction scheme and heterogeneous loss parameters can be found in the appendices, Tables A1–A5.

$$-\frac{\mathrm{d[X]}}{\mathrm{d}t}=k_u[\mathrm{X}] \qquad k_u=\frac{\varpi A{:}\gamma}{4} \qquad w=\sqrt{\frac{8RT}{\pi \mathrm{M}}} \qquad (1)$$

where k_u is the uptake rate coefficient, A is the aerosol volumetric surface area, γ is the reactive uptake coefficient, ϖ is the mean molecular speed of molecule X, R is the molar gas constant, T (K) is the ambient temperature and M is the molar mass.

3 Results and discussion

3.1 Overview of LIF IO measurements

The LIF instrument measured throughout the field campaign for a period of 20 days (7 September to 28 September 2008), see Fig. 3. Night-time measurements were made on four nights. IO was observed above the instrument limit of detection (0.4–4 pptv for a 150 s integration period, see Sect. 2.2) on 14 days (when no negative bias of the signal was observed, see Sect. 3.3), of which a clear diurnal profile was observed on 11 days; the maximum daytime IO detected was 30.0±7.1 pptv (10 s integration period). IO concentrations were below the instrument's limit of detection or highly scattered around zero on the remaining days. There were three periods during the campaign when IO was not detected, which can be explained by a combination of lack of macroalgae exposure (neap tides) or meteorological conditions, as discussed below. Night-time IO was detected on two of the four nights of measurements, at mixing ratios of 1.1–2.0 pptv (60 min average).

The important influences on IO concentrations at the Roscoff site were found to be tidal height, solar irradiation, wind direction, wind speed and levels of NO_x. These will be discussed in the next section.

3.2 Influences on daytime IO concentrations

The concentration of IO at Roscoff was strongly dependent on tidal height and the intensity of solar irradiation, consistent with previous studies at similar locations and providing further evidence that the source of IO originates from emissions of iodine species from macroalgae beds that are exposed as the tide retreats (Peters et al., 2005, Saiz-Lopez et al., 2006b). The subsequent detection of IO was also dependent on meteorological conditions due to the LIF instrument being positioned at a distance from the iodine source (Fig. 1). Measurements of IO by LP-DOAS and multi-axis DOAS (MAX-DOAS) in the Gulf of Maine, where the island shores are populated with kelp, including the *Laminaria* species, did not show a tidal dependence (Stutz et al., 2007), emphasizing that not all coastal environments provide identical conditions.

IO concentrations (pptv) in the daytime displayed a clear anti-correlation with tidal height (*TH*, m), as displayed in Fig. 4. The best fit expression to an exponential decay gave:

$$[IO]=10.05\exp^{(-TH/2.80)}-0.34,\ R^2=0.90 \tag{2}$$

where R^2 is the statistical measure of how well the exponential decay approximates the data points. A second order polynomial and linear expressions also provide fits of similar confidence, however, (R^2=0.89 and R^2=0.90, respectively) which illustrates that several mathematical dependencies may be used to describe the relationship. When comparing the second order polynomial dependence of daytime IO (pptv) on tidal height (m) to the same expression calculated by Peters et al. (2005) at Lilia, a coastal site ~40 km west of Roscoff, the expressions are similar, indicating that the IO production pathway may be similar at both locations:

$$\text{Roscoff}, [IO]=0.11\times TH^2-1.90\times TH+8.10 \tag{3}$$

$$\text{Lilia}, [IO]=0.13\times TH^2-1.95\times TH+7.28 \tag{4}$$

Solar irradiation is also essential for the production of IO because the production of IO results from the photolysis of iodine species; Fig. 5 shows the correlation that exists between IO concentrations and $j(I_2)$. The photolysis of I_2 to produce two I atoms has a relatively broader, flatter profile compared to the photolysis of O_3 to produce $O(^1D)$ atoms, another important photochemical reaction resulting in the production of OH, due to the broad absorption of I_2 across the UV and visible spectrum, with a maximum absorption located between 500–600 nm (Saiz-Lopez et al., 2004). Overall, IO was found to have a stronger dependence on tidal height compared to solar irradiation. This suggests that the IO concentration is more dependent on the macroalgal source of iodine compounds than the availability of solar radiation. The clearest examples of the domination of tidal height rather than solar irradiation is provided by studying two days of the campaign when the tidal minimum occurs at a different time of day (Fig. 6). The 8 September was a clear day, providing a flat $j(I_2)$ profile throughout the day once it had risen from zero at dawn, yet the IO displays a large variation around the tidal minimum. The wind prevailed from macroalgae area A (Fig. 1). On 14 September solar irradiation was more variable and low tide fell late in the afternoon (wind prevailed from just north of macroalgae area C). On both of these days IO peaked at the tidal minimum. On 14 September, IO did not peak at solar noon.

Wind speed and direction also influenced IO concentrations, see Fig. 7. We hypothesise that an air parcel must travel over an I_2 emitting bed of macroalgae in order for IO to be detected by the LIF instrument. It also seems likely that the wind speed must be sufficiently high to transport IO to the LIF instrument before it is lost by chemical or physical removal (we return to this point in the subsequent sections).

Towards the end of the campaign, when IO levels returned to high values, the wind prevailed from the west to south west, where the macroalgae beds were located at a greater distance compared to northwest to easterly winds which prevailed earlier in the campaign (over 1000 m compared to 300 m, see Fig. 1). This suggests that IO can be sustained as it is transported from more remote macroalgae beds (discussed further in Sect. 3.3).

The point source measurements of IO at the field site by the LIF instrument display an anti-correlation with point source NO_x measurements (measured by the University of York chemiluminescent NO and NO_2 instrument adjacent to the LIF instrument; see McFiggans et al., 2009, for details), as illustrated in Fig. 8. High concentrations of IO were not observed when NO_x concentrations were high (NO_2 concentrations were generally between 1–5 ppbv during the campaign), even at low tide, in contrast to IO measurements at Appledore Island, where NO_2 was between 5–10 ppbv (Stutz et al., 2007). A time-series of highly time-resolved IO (10 s time resolution) and NO_2 (Fig. 9) allows short-timescale variations in the concentrations of these gases to be resolved. During mid-morning (10:30 GMT), when photolysis rates were increasing and tidal height was decreasing, there was a period of nearly 20 min when IO concentrations were suppressed, corresponding to a substantial NO_2 spike of 2.1 ppbv. There is similar evidence for this later in the day but this also corresponds to a drop in $j(I_2)$. These two variables that influence IO cannot be differentiated in the latter example. Throughout this day, the wind direction remained unchanged, although the airmass trajectory may have altered prior to sampling. In the presence of NO_x, I atoms and IO react to form the reservoir species INO_2, $IONO_2$ and INO (Reactions R10–R12). The reaction of NO with IO results in the release of reactive I atoms (Reaction R13).

$$I+NO_2+M \rightarrow INO_2+M \tag{R10}$$

$$IO+NO_2+M \rightarrow IONO_2+M \tag{R11}$$

$$I+NO+M \rightarrow INO+M \tag{R12}$$

$$IO+NO \rightarrow I+NO_2 \tag{R13}$$

$$OIO+NO \rightarrow IO+NO_2 \tag{R14}$$

Model simulations were performed to explore the IO – NO_x dependence. The MCM model was run using typical daytime conditions, with an injection of 100 pptv I_2 at the start of the run. During the campaign, the LP-DOAS instrument measured up to ~26 pptv daytime I_2 and the BBCRDS instrument measured up to ~70 pptv. I_2 levels were assumed to be higher than these measurements at the point of emission. NO_x concentrations were varied from 0–10 ppbv (ratio NO_2:NO=4:1). All species were allowed to vary apart from O_2, N_2 and H_2O which were kept constant. The modelled [IO] after 50 s (solid red) and 60 s (dashed red) time evolution are shown in Fig. 8 and present the best fit to the observed data. As is evident in the plot, the modelled IO also displays an anti-correlation with NO_x (exponential decay fit, $[IO]=1.00+11.8{:}\exp(-[NO_x]/2.40)$, $R^2=0.997$ at t=50 s and

$[IO]=0.98+9.02{:}\exp(-[NO_x]/2.49)$, $R^2=0.996$ at t=60 s), although the modelled IO decays are shallower than the observed decay with respect to $[NO_x]$. The modelled anti-correlation exists because NO_x acts to suppress IO primarily through the formation of $IONO_2$ (Reaction R11). The impact of NO is lower than NO_2; $IONO_2$ and INO_2 were found to act as a greater IO reservoir compared to INO. NO (I) reacts with IO directly (resulting in the release of I atoms which can subsequently react with O_3 to produce IO, Reaction R22) and (II) indirectly reduces IO by reaction with its I atom precursor (Reaction R12). NO is also involved in the release of IO via reaction with OIO (R14).

Kaltsoyannis and Plane (2008) recently proposed that at $IONO_2{:}O_3>0.01$, I atoms will preferentially react with $IONO_2$ (Reaction R15) rather than O_3 (Reaction R2) limiting the build up of this reservoir species and helping maintain IO concentrations in high NO_x environments. Mahajan et al. (2009) have found that the inclusion of this recycling mechanism was necessary to reproduce I_2/IO ratios observed by LP-DOAS at Roscoff during the RHaMBLe campaign using a 1-D model. Inclusion of this recycling mechanism in the 0D model used in this work reduces the anti-correlation observed between IO and NO_x. The modelled gradient becomes shallower still when the time between emission and sampling is increased further (the transit times from the major seaweed beds, highlighted in Fig. 1, to the LIF inlet ranged from less than 100 s to greater than 600 s).

$$I+IONO_2 \rightarrow I_2+NO_3 \qquad \text{(R15)}$$

Therefore, the anti-correlation of IO versus NO_x observed may not be caused solely by chemical reactions between IO and NO_x. Rather, the relationship could be due also to the spatial heterogeneity of macroalgae and NO_x sources (a point further discussed in McFiggans et al., 2009). Little or no IO was observed whenever the wind prevailed from the town (Fig. 7) as no seaweed beds lay in this direction. Under such conditions NO_x concentrations were elevated due to anthropogenic emissions, lending to an apparent anti-correlation. This IO-NO_x relationship resolved by comparison of two point source techniques may not be discernible when comparing spatially averaged IO and

NO_2 measured by LP-DOAS instruments (e.g. Stutz et al., 2007) as spatial averaging will smooth out (to a certain extent) the heterogeneity of the IO and NO_x sources.

3.3 Measurements of IO at night

During the campaign the LIF instrument detected IO on two of four nights of measurements, around the tidal minimum, at mixing ratios of 1–2 pptv (Fig. 10). On these nights the wind direction corresponded to a near (300 m) (8–9 September) or far (2800 m) (25–26 September) source of I_2. An analysis of the Gaussian distribution of the deviation of the online and offline signal from the mean of the offline signal confirms that the signal is positive around the tidal minimum on 8–9 September and 25–26 September. The results of this analysis on 8–9 September show that there is a clear positive signal between 00:00–02:00, compared to 23:00–00:00 and 02:00–03:00, when both online and offline signals correspond to zero (Fig. 11). During the campaign the LP-DOAS instrument detected IO on three out of eight nights of measurements at up to 3.0±0.9 pptv. The night of the 8th is the only night when both the LIF and LP-DOAS instruments were operated together; on this night both instruments detected comparable levels of IO around low tide. These results provide further evidence that there is a non-photolytic source of IO, such as via reaction:

$$I_2+NO_3 \rightarrow I+INO_3 \qquad \text{(R16)}$$

followed by:

$$I+O_3 \rightarrow IO+O_2 \qquad \text{(R17)}$$

The proposed precursors of night-time IO were detected at the Roscoff site. Up to 52 pptv I_2 was detected by LP-DOAS (Mahajan et al., 2009) and 40–80 pptv (NO_3+N_2O_5) was detected by BBCEAS (Langridge et al., 2008). These measurements were not made on the same nights as the LIF IO measurements. Optimal conditions for NO_3 formation at night are significant levels of NO_2 combined with low NO concentrations, due to the rapid removal of NO_3 via reaction with NO. On the nights IO was detected, NO was below 0.12 ppbv and NO_2 was 2.25 to 2.42 ppbv.

A photochemical box model was used to examine these results (model described in Sect. 2.3). Each model run was initiated with estimated I_2, NO_3, CH_3I, CH_2IBr and DMS, and ambient measurements of NO, NO_2 and O_3 (measured close to the LIF container) and are summarised in Table 1. Concentrations of the species listed in Table 1 and temperature (288 K) were constant throughout the model run, once initiated. The model was initiated at 23:00 and run to steady state IO conditions.

The model was run for the two separate nights when IO was detected by the LIF instrument, resulting in an under prediction of IO on both nights. The measured/modelled IO ratio varied from 3–6. This ratio was used as a scaling factor to adjust I_2 levels. I_2 levels were increased from 50 pptv to 150 and 320 pptv for the two nights respectively. This resulted in an excellent measured/modelled agreement of 1.08 and 1.02. The higher scaling factor on the night of 25-26 September corresponds to meteorological conditions that bring iodine species from macroalgae beds further from the measurement site compared to 8–9 September. The higher IO levels detected on the night of 25 – 26th are unexpected considering the source is further away compared to 8–9 September (according to the macroalgae bed survey). This indicates a stronger iodine source, such as larger or more active macroalgae beds and suggests that the model failure is due to an insufficient quantity of initial I_2. It can be inferred that the I_2 concentration at the macroalgae bed was higher than that measured by LP-DOAS (and remained higher during transport to the LIF inlet); elevated point measurements of I_2 detected by BBCRDS close to the LIF inlet (Leigh et al., 2009) support this hypothesis.

3.4 Comparison of IO measurement techniques

The RHaMBLe-Roscoff campaign was unique because it provided simultaneous, closely located measurements of IO by four different instruments. These were the LIF (University of Leeds; Whalley et al., 2007); LP-DOAS (University of Leeds, Mahajan et al., 2009); Concurrent Multi Axis DOAS (CMAX-DOAS) (University of Leicester;

Leigh et al., 2006) and Cavity Ringdown Spectroscopy (CRDS) (University of Bristol; Wada et al., 2007) instruments. Each instrument provided a different measurement footprint. DOAS instruments provide spatially averaged measurements and have been deployed to measure IO at a variety of sites. The most recent review of IO measurements can be found in von Glasow and Crutzen (2007). The addition of novel LIF and CRDS instruments provide point-source measurements, enabling a greater interpretation of iodine chemistry at this site, for example the extent of the spatial heterogenity (or hot-spots) of the iodine sources. The LIF instrument also provided a high temporal resolution (10 s integration period during this field campaign), which reveals the high temporal variability of IO (see Fig. 9) possibly caused by fast fluctuations in the concentrations of other trace gases, for example I_2 or NO_x, changes in meteorological conditions (wind speed, wind direction, solar irradiation) or changes in the exposure of macroalgae beds as the tide retreats.

The LP-DOAS instrument provided measurements over an average of a 6.7 km light path at a height of 7 to 12 m above the mean sea level (Fig. 1). IO was retrieved in a 425–445 nm spectral window, which also includes NO_2 and H_2O. The CMAX-DOAS provided slant column measurements (telescopes pointing 2° and 5° N, 5° E and 5° W; viewing angles above the horizon) using a retrieval window between 434 and 459 nm, to include the absorption bands of IO at 436, 445 and 456 nm, further details can be found in McFiggans et al. (2009). The LIF, CRDS and CMAX-DOAS instruments were all located within ~7 m of each other (Fig. 2). The LP-DOAS instrument was located ~25 m from the other instruments. A comparison of the four instruments is given in Table 2.

During the RHaMBLe-Roscoff field campaign the LIF IO and LP-DOAS instruments were measuring IO simultaneously on seven days. When both instruments were measuring simultaneously, there was never an instance of IO detection by the LIF instrument and not the LP-DOAS instrument. Meteorological and NO_x conditions on 8 September and 9 September were similar but IO concentrations measured by the two instruments were very different. The 17 September is an example of positive detection of IO by the LP-DOAS instrument in the absence of detection by the LIF IO instrument. CMAX-DOAS measurements are also used to give information about the spatial IO distribution, but the CRDS measurements are not considered due to the small number of coincident observations made.

3.4.1 8 September and 9 September 2006

During the 8 September to 9 September meteorological conditions were similar. Winds were easterly (corresponding to macroalgae area A, Fig. 1) and wind speeds were relatively high. Photolysis rates were similar on both days. The tidal range was at a maximum (spring tide) with low tide around midday. Five day back trajectory analysis shows that the air mass was North Sea in origin, approaching from the east and descending over France. On the 9 September the air mass approached the site from a slightly more south east direction, with slightly lower wind speeds (4–5 $\mathrm{ms^{-1}}$ compared to 5.5–6.5 $\mathrm{ms^{-1}}$, measured at the LIF container). Concentrations of NO were 0.18 and 0.22 ppbv. An increase of ~50% from 0.54 to 0.82 ppbv was observed in NO_2 from 8 September to 9 September (average concentrations for a period of one hour around peak IO). The LP-DOAS NO_2 measurement was twice that on the 9 September compared to the 8th September (0.7 to 1.5 ppbv, 10:00–14:00).

The IO diurnal profiles are displayed together in Fig. 12, and as a ratio in Fig. 13. The LP-DOAS measurements display a lower degree of variability compared to the LIF measurements, resulting from the 3.35 km path length that the LP-DOAS measurements are averaged over, resulting in measured IO being smoothed out spatially. The measurements show that on 8 September the LIF IO instrument measured approximately twice that of the LP-DOAS instrument. However, on 9 September both instruments measured approximately the same peak concentrations. On both days, the ratio of LIF IO:LP-DOAS IO increases after low tide, indicating that the LIF instrument observes higher concentrations of IO for a longer time period, later in the day.

This relationship can be explained by examining the spatial distribution of macroalgae and the air mass transport time from source region to the LIF instrument or

LP-DOAS light path. On the 9 September the air mass was approaching from a slightly more south easterly direction, thus passing over fewer macroalgae beds (see Fig. 1). The lower wind speed on the 9 September increases the time taken for the airmass to travel from the macroalgae to the LIF measurement point, resulting in a greater decay of IO, which may be why the LIF instrument measures lower [IO] (compared to 8 September). The larger spatial coverage provided by the LP-DOAS instrument enables interception from a greater number of macroalgae areas, resulting in [IO] similar to LIF measurements.

Further insight into the LIF:LP-DOAS relationship can be gained by studying CMAX-DOAS measurements of IO. The CMAX-DOAS and LIF instruments observed the same daily variation in IO concentrations (Fig. 14), both instruments detecting higher levels of IO on 8 September. Like LIF measurements, CMAX-DOAS IO persists longer after peak IO compared to LP-DOAS measurements. On 8th September, the 5° N CMAX-DOAS telescope observed higher concentrations of IO compared to the westerly telescope. On 9 September, comparison of CMAX-DOAS 5° N and W telescope IO measurements indicate a stronger source of IO from the north/east, resulting from an easterly wind direction. This implies that the ∼1:1 ratio of LIF to LP-DOAS measurements on 9 September is because the LP-DOAS instrument is more responsive to this northerly/easterly source compared to the LIF and CMAX-DOAS instruments.

3.4.2 17 September 2006

The 17 September provides an example of the positive detection of IO by LP-DOAS with corresponding LIF measurements of IO close to the instrument's detection limit (Fig. 15). No other IO instrumentation was operating on this day. The LP-DOAS instrument detected 6.8±2.4 pptv of IO, around low tide. The LIF instrument detected very low concentrations close to the detection limit (0.5–0.6 pptv, 1000 s integration period) with a possible positive peak just after low tide on 17 September (upper limit 2.1 pptv). The LIF instrument did not detect IO because of the low tidal range, and low tide fell in the morning when solar irradiation was low. Additionally, a combination of medium strength winds (2.5–3.5 $\mathrm{m\,s^{-1}}$) prevailing from macroalgae beds which were far from the LIF instrument (over 1 km; Fig. 1, area C) result in the requirement for a long time period to sustain IO levels (over ∼330 s from macroalgae bed to LIF cell). The long path length of the LP-DOAS instrument means that it can detect IO over a wider region, which can provide a footprint that includes more macroalgae beds (compared to the point source LIF instrument), e.g. macroalgae beds that are very distant (upwind) of the LIF instrument.

The measurement of differing IO mixing ratios by LIF compared to spatially averaged techniques (DOAS) provides strong evidence that IO is not uniformly distributed at Roscoff, an environment where the major source of iodine species are macroalgae. The LIF/LP-DOAS ratio was not constant and was dependent on meteorological conditions and the distribution of macroalgae at the field site.

3.5 Particle formation and iodine oxides

IO is an essential precursor to the iodine-mediated proposed reaction mechanism for the production of ultra-fine particles, therefore coordinated in situ measurement of both may enable a better understanding of their relationship. The results from this campaign provide 18 days when co-located IO and particle counter instruments were operating (located ∼15 m apart; see Fig. 2). Measurements of particle number above diameter 2.5 nm (3.0 nm from 11 September) and 10 nm were made using Condensation Particle Counters (TSI models UCPC 3776 – 2.5 nm, UCPC 3025AS – 3 nm, and CPC 3010AS – 10 nm) by the University of Manchester (Whitehead et al., 2009). The difference between the two measurements provided a number count in the 2.5 nm (or 3.0 nm) – 10 nm diameter range. The campaign time series is shown in Fig. 16. The results show that ultrafine particle events (2.5 nm<diameter (d)<10 nm) correlate with elevated concentrations of IO. There is one anomalous day (15 September), when IO concentrations are elevated yet there is an absence of particles. Figure 17 shows a correlation plot of peak particle number (2.5 nm<d<10 nm) versus peak IO for the

18 days of coincident measurements, which displays a positive correlation (linear fit; see Fig. 17 for details). This provides direct evidence that the nucleation source of particle bursts at Roscoff and other similar marine environments is proportional to IO. The data points in Fig. 17 originate from a variety of macroalgae source regions (both close to and further from the measurement point), assuming that IO and particles are from the same I_2 source regions, the correlation between particle number and IO concentration provides evidence that the I atom/IO couplet is quite persistent despite the short IO photolysis lifetime; this coupling efficiently buffers the IO concentration and preserves the particle vs. IO correlation. As shown in Fig. 18, the IO concentration displayed a broader profile compared to particle number, IO tended to increase between 75 to 160 min before particle number increased and fell up to 75 min after particle number had fallen. There was, however, some variability in the temporal profile of each species, for example, when the wind direction corresponded to an iodine source close to the measurement site (Fig. 1, area A) the rise in IO was rapid and particle number increased from background levels earlier; observed on 8 September (Fig. 18). On the days when the iodine source was further from the field site (areas B and C), and the rise in IO concentration was slower, the rise in particle number begins later (relative to the rise in IO), such as observed on 7 September. Particle formation is at least second order in OIO, and, therefore, at least 4 September order in IO. As a consequence of this, at the lower IO concentrations the particle production potential will be extremely small, as IO concentrations increase, the particle production potential becomes measurable, lending to the much broader IO profile observed relative to the particle number profile. These results provide direct evidence that IO is involved in the mechanism of new particle formation at coastal sites and supports the link between photochemical O_3 destruction and particle formation at marine locations, discussed further in Whitehead et al. (2009).

4 Modelling study: impact of iodine chemistry on daytime HO_x levels

The dominant daytime oxidant, OH, is closely coupled to HO_2 through reactions with trace gases. In polluted environments HO_2 is converted to OH via reaction with NO (Reaction R18). In low NO environments, the conversion of HO_2 to OH proceeds via reaction with O_3 (Reaction R19). The presence of halogen monoxides (XO, where X=I or Br or Cl) provides an alternative two step route for HO_2 to OH conversion (Reactions R20 and R21). Previous modelling studies (Davis et al., 1996, Stutz et al., 1999, Bloss et al., 2005, Bloss et al., 2007, Read et al., 2008, Whalley et al., 2009) have found that the presence of iodine species leads to an enhancement of OH due to the conversion of HO_2 to OH via reaction with IO. In contrast, Keene et al. (2009) found that OH concentrations decreased in the presence of ClO due to an increase in oxidation of NO_x and corresponding reduction in Reaction R18. Here we consider the impact of IO only on HO_x levels.

$$HO_2+NO \rightarrow OH+NO_2 \tag{R18}$$

$$HO_2+O_3 \rightarrow OH+2O_2 \tag{R19}$$

$$HO_2+XO \rightarrow HOX+O_2 \tag{R20}$$

$$HOX+h\nu \rightarrow OH+X \tag{R21}$$

A photochemical box model (see Sect. 2.3 and appendices for full mechanism) has been used to investigate the effect of iodine chemistry on HO_x concentrations under different NO_x conditions, relevant to the RHaMBLe-Roscoff campaign when reasonably high levels of NO_x (1–5 ppbv) were experienced due to the close proximity of the measurement site to the town. Model calculations for four different NO_x scenarios were run (zero, low, medium and high NO_x concentrations), representative of conditions experienced during the campaign. The model was initiated at midnight and run to noon time steady state HO_x conditions. Concentrations of NO, NO_2, CO, CH_4, non-methane hydrocarbons (C2–C4), O_3, CH_3I, CH_2IBr and IO and uptake coefficients onto aerosol (Table A5) were kept constant. This allowed the effect of iodine chemistry on HO_x to be evaluated under different IO loadings.

A baseline zero NO_x scenario was run as a comparison case. As expected, increasing IO results in an increase of OH at the expense of HO_2, via Reactions R20 and R21, decreasing the $[HO_2]/[OH]$ ratio (Fig. 19). As NO_x concentrations increase, the influence of iodine chemistry on HO_x decreases. The presence of IO in a low NO_x scenario (NO=0.075 ppbv, NO_2=0.357 ppbv) results in the enhancement of OH up to a critical point of IO=15 pptv. Above these IO levels, OH levels decrease. The critical IO concentration decreases as NO_x increases until a point when the presence of IO always results in a decrease of OH.

A rate of production analysis shows that in a low NO_x environment the conversion of HO_2 to OH via IO (Reactions R20 and R21) is always greater than via NO (Reaction R18) and the Reactions R22 and R23 are slow. Under high NO_x conditions, the conversion of HO_2 to OH via NO dominates. The presence of IO suppresses Reaction R18 by reaction of IO with NO and NO_2 (Reactions R22 and R23).

$$IO+NO \rightarrow I+NO_2 \tag{R22}$$

$$IO+NO_2+M \rightarrow IONO_2+M \tag{R23}$$

The high concentrations of IO measured at Roscoff (up to 30 pptv) under variable NO_x concentrations will impact local air quality by impacting the local OH and HO_2 levels. As NO_x concentrations increase OH to HO_2 conversion becomes less significant, until the presence of IO results in a decrease of OH. The presence of halogens can actually decrease the oxidative capacity of the atmosphere at the higher NO_x concentrations experienced.

5 Conclusions

The results presented from the RHaMBLe-Roscoff campaign represent the first measurement of ambient IO by LIF. From 20 days of measurements, IO was observed above the instrument limit of detection on 14 days, of which a clear diurnal profile was observed on 11 days. IO concentrations were below the instrument's limit of detection or highly scattered around zero on the remaining days. The maximum IO measured was 30.0 pptv over a 10 s integration period (limit of detection =1.4 pptv for 10 s). A strong dependence of IO concentrations on tidal height was found. Additionally, the main influences on IO concentrations were the intensity of solar irradiation, wind direction and wind speed. This cements confidence in the hypothesis that the source of IO is emission of halogen species from macroalgae when the latter are exposed during low tide. During the day, solar irradiation is necessary to provide a photolytic source of I atoms. The night-time measurements of IO during this study provide further evidence of a non-photolytic source of IO via reaction of I_2 with NO_3 (Chambers et al., 1992).

A comparison of point source and spatially averaged IO measurements show that point source LIF measurements can be at least twice that of spatially averaged LP-DOAS measurements. This provides strong evidence that IO is not uniformly distributed in an environment where the major source of iodine species are macroalgae. IO concentrations detected by the LIF instrument represent a more applicable constraint in modelling studies when the supporting measurements are also point sources. The practice of scaling up IO measured using LP-DOAS to account for hot-spots of IO along the light path is verified by the comparisons between LIF-IO and LP-DOAS-IO presented here. The LIF/LP-DOAS ratio was not constant, however, and was found to be dependent on meteorological conditions and the distribution of macroalgae at the field site, demonstrating that care must be exercised when converting LP-DOAS data to a point source model constraint. At this site, the LP-DOAS instrument detected IO sourced from a northerly/easterly direction with greater ability than the LIF instrument. This indicates the advantage of LP-DOAS compared to LIF to detect IO when the source is at a greater distance than the IO lifetime, or when a larger measurement footprint is required. The combination of point source and spatially averaged measurements improves the ability to interpret halogen chemistry. In the future, a mobile I_2 or IO instrument would provide an excellent way to measure the concentration of these species directly at the macroalgae beds, thus providing greater measurement of the spatial gradient of I_2 and IO.

Ultra fine particles were found to strongly correlate with IO measured by LIF, providing further evidence that coastal new particle events are due to emission of iodine species from macroalgae via formation pathways involving IO.

A modelling study concludes that at coastal environments such as Roscoff the presence of IO via the exposure of macroalgae has significant impacts on the local HO_x levels. Under low NO_x conditions, the presence of IO increases OH levels and the oxidative capacity of the atmosphere, but as NO_x concentrations increase the presence of IO eventually results in a decrease of OH. Iodine was found to decrease the oxidative capacity of the atmosphere at the higher NO_x concentrations experienced during the campaign.

Acknowledgements. The authors would like to thank P. Pontin (Station Biologique de Roscoff, France) for organisational and logistical support prior to and throughout the RHaMBLe-Roscoff field campaign, and for the provision of the raw bathymetry data and seaweed mapping used to produce the macroalgae map. R. Dunk (Crichton Carbon Centre, formerly University of York) is acknowledged for providing the tidal height data. Thanks also to the University of Leeds, School of Chemistry mechanical and electronic workshops for their help in construction of the LIF IO instrument. We thank NERC for the award of studentship to KLF. ASM acknowledges a University of Leeds studentship.

References

Alicke, B., Hebestreit, K., Stutz, J., and Platt, U.: Iodine oxide in the marine boundary layer, Nature, 397, 572–573, 1999. 25740

Allan, B., McFiggans, G., Plane, J., and Coe, H.: Observations of iodine monoxide in the remote marine boundary layer, J. Geophys. Res, 105, 14363–14369, 2000. 25740

Atkinson, R., Baulch, D. L., Cox, R. A., Crowley, J., Hampson, R. F., Kerr, J. A., Rossi, M., and Troe, J.: Summary of evaluated kinetic and photochemical data for atmospheric chemistry, Tech. Rep., 2002. 25775

Atkinson, R., Baulch, D., Cox, R., Crowley, J., Hampson, J. R., Kerr, J., Rossi, M., and Troe, J.: Summary of evaluated kinetic and photochemical data for atmospheric chemistry, IUPAC Subcommittee on Gas Kinetic Data Evaluation for Atmospheric Chemistry, 2004. 25777

Atkinson, R., Baulch, D. L., Cox, R. A., Crowley, J. N., Hampson, R. F., Hynes, R. G., Jenkin, M. E., Rossi, M. J., and Troe, J.: Evaluated kinetic and photochemical data for atmospheric chemistry: Volume III - gas phase reactions of inorganic halogens, Atmos. Chem. Phys., 7, 981–1191, 2007, http://www.atmos-chem-phys.net/7/981/2007/. 25774, 25776, 25777

Bloss, W. J., Lee, J. D., Johnson, G. P., Sommariva, R., Heard, D. E., Saiz-Lopez, A., Plane, J. M. C., McFiggans, G., Coe, H., Flynn, M., Williams, P., Rickard, A. R., and Fleming, Z. L.: Impact of halogen monoxide chemistry upon boundary layer OH and HO$_2$ concentrations at a coastal site, Geophys. Res. Lett., 32, L06814, doi:10.1029/2004GL022084, 2005. 25740, 25759

Bloss, W. J., Lee, J. D., Heard, D. E., Salmon, R. A., Bauguitte, S. J.-B., Roscoe, H. K., and Jones, A. E.: Observations of OH and HO$_2$ radicals in coastal Antarctica, Atmos. Chem. Phys., 7, 4171–4185, 2007, http://www.atmos-chem-phys.net/7/4171/2007/. 25759

Burkholder, J. B., Curtius, J., Ravishankara, A. R., and Lovejoy, E. R.: Laboratory studies of the homogeneous nucleation of iodine oxides, Atmos. Chem. Phys., 4, 19–34, 2004, http://www.atmos-chem-phys.net/4/19/2004/. 25742

Cainey, J. M., Keywood, M., Grose, M. R., Krummel, P., Galbally, I. E., Johnston, P., Gillett, R. W., Meyer, M., Fraser, P., Steele, P., Harvey, M., Kreher, K., Stein, T., Ibrahim, O., Ristovski, Z. D., Johnson, G., Fletcher, C. A., Bigg, E. K., and Gras, J. L.: Precursors to Particles (P2P) at Cape Grim 2006: campaign overview, Environ. Chem., 4, 143–150, 2007. 25740

Title Page
Abstract | Introduction
Conclusions | References
Tables | Figures
◀| |▶
◀ ▶
Back | Close
Full Screen / Esc
Printer-friendly Version
Interactive Discussion

Chambers, R. M., Heard, A. C., and Wayne, R. P.: Inorganic Gas-Phase Reactions of the Nitrate Radical: I_2+NO_3 and I + NO_3, J. Phys. Chem., 96, 3321–3331, 1992. 25740, 25761, 25774

Cox, R. A., Bloss, W. J., Jones, R. L., and Rowley, D. M.: OIO and the Atmospheric Cycle of Iodine, Geophys. Res. Lett., 26, 1857–1860, 1999. 25742

Davis, D., Crawford, J., Liu, S., McKeen, S., Bandy, A., Thornton, D., Rowland, F., and Blake, D.: Potential impact of iodine on tropospheric levels of ozone other critical oxidants, J. Geophys. Res., 101, 2135–2147, 1996. 25740, 25759

Dillon, T. J., Tucceri, M. E., Sander, R., and Crowley, J. N.: LIF studies of iodine oxide chemistry, Phys. Chem. Chem. Phys., 10, 1540–1554, 2008. 25774

Gilfedder, B. S., Lai, S. C., Petri, M., Biester, H., and Hoffmann, T.: Iodine speciation in rain, snow and aerosols, Atmos. Chem. Phys., 8, 6069–6084, 2008, http://www.atmos-chem-phys.net/8/6069/2008/. 25742

Gomez Martin, J. C., Spietz, P., and Burrows, J. P.: Kinetic and Mechanistic Studies of the I_2/O_3 Photochemistry, J. Phys. Chem. A, 111, 306–320, doi:10.1021/jp061186c, 2007. 25774

Gomez Martin, J. C., Ashworth, S. H., Mahajan, A. S., and Plane, J. M. C.: The photochemistry of OIO: laboratory study and atmospheric implications, Geophys. Res. Lett., 36, L09802, doi:10.1029/2009GL037642, 2009. 25743, 25777

Gravestock, T., Blitz, M. A., and Heard, D. E.: Kinetics study of the reaction of iodine monoxide radicals with dimethyl sulfide, Phys. Chem. Chem. Phys., 7, 2173–2181, 2005. 25774

Heard, D. E., Read, K. A., Methven, J., Al-Haider, S., Bloss, W. J., Johnson, G. P., Pilling, M. J., Seakins, P. W., Smith, S. C., Sommariva, R., Stanton, J. C., Still, T. J., Ingham, T., Brooks, B., De Leeuw, G., Jackson, A. V., McQuaid, J. B., Morgan, R., Smith, M. H., Carpenter, L. J., Carslaw, N., Hamilton, J., Hopkins, J. R., Lee, J. D., Lewis, A. C., Purvis, R. M., Wevill, D. J., Brough, N., Green, T., Mills, G., Penkett, S. A., Plane, J. M. C., Saiz-Lopez, A., Worton, D., Monks, P. S., Fleming, Z., Rickard, A. R., Alfarra, M. R., Allan, J. D., Bower, K., Coe, H., Cubison, M., Flynn, M., McFiggans, G., Gallagher, M., Norton, E. G., O'Dowd, C. D., Shillito, J., Topping, D., Vaughan, G., Williams, P., Bitter, M., Ball, S. M., Jones, R. L., Povey, I. M., O'Doherty, S., Simmonds, P. G., Allen, A., Kinnersley, R. P., Beddows, D. C. S., Dall'Osto, M., Harrison, R. M., Donovan, R. J., Heal, M. R., Jennings, S. G., Noone, C., and Spain, G.: The North Atlantic Marine Boundary Layer Experiment(NAMBLEX), Overview of the campaign held at Mace Head, Ireland, in summer 2002, Atmos. Chem. Phys., 6, 2241–2272, 2006, http://www.atmos-chem-phys.net/6/2241/2006/. 25743

Hoffmann, T., O'Dowd, C. D., and Seinfeld, J. H.: Iodine oxide homogeneous nucleation: An explanation for coastal new particle formation, Geophys. Res. Lett., 28, 1949–1952, 2001. 25740, 25742

Jacob, D. J.: Heterogeneous chemistry and tropospheric ozone, Atmos. Environ., 34, 2131–2159, 2000. 25778

Jenkin, M. E., Saunders, S. M., and Pilling, M. J.: The tropospheric degradation of volatile organic compounds: A protocol for mechanism development, Atmos. Environ., 31, 81–104, 1997. 25746

Jenkin, M. E., Saunders, S. M., Wagner, V., and Pilling, M. J.: Protocol for the development of the Master Chemical Mechanism, MCM v3 (Part B): tropospheric degradation of aromatic volatile organic compounds, Atmos. Chem. Phys., 3, 181–193, 2003, http://www.atmos-chem-phys.net/3/181/2003/. 25746

Jimenez, J. L., Bahreini, R., Cocker III, D. R., Zhuang, H., Varutbangkul, V., Flagan, R. C., Seinfeld, J. H., O'Dowd, C. D., and Hoffman, T.: New particle formation from photooxidation of diiodomethane (CH_2I_2), J. Geophys. Res., 108(D10), 4318, 2003. 25742

Joseph, D. M., Ashworth, S. H., and Plane, J. M. C.: On the photochemistry of $IONO_2$: absorption cross section (240–370 nm) and photolysis product yields at 248 nm, Phys. Chem. Chem. Phys., 9, 5599–5607, 2007. 25777

Kaltsoyannis, N. and Plane, J. M. C.: Quantum chemical calculations on a selection of iodine-containing species (IO, OIO, INO_3, $(IO)_2$, I_2O_3, I_2O_4, and I_2O_5) of importance in the atmosphere, Phys. Chem. Chem. Phys., 10, 1723–1733, 2008. 25740, 25742, 25751, 25773

Kanaya, Y., Yokouchi, Y., Matsumoto, J., Nakamura, K., Kato, S., Tanimoto, H., Furutani, H., Toyota, K., and Akimoto, H.: Implications of iodine chemistry for daytime HO_2 levels at Rishiri Island, Geophys. Res. Lett., 29, 1212, doi:10.1029/2001GL014061, 2002. 25741

Keene, W. C., Long, M. S., Pszenny, A. A. P., Sander, R., Maben, J. R., Wall, A. J., O'Halloran, T. L., Kerkweg, A., Fischer, E. V., and Schrems, O.: Latitudinal variation in the multiphase chemical processing of inorganic halogens and related species over the eastern North and South Atlantic Oceans, Atmos. Chem. Phys. Discuss., 9, 11889–11950, 2009, http://www.atmos-chem-phys-discuss.net/9/11889/2009/. 25759

Kulmala, M., Pirjola, L., and Makela, J. M.: Stable sulphate clusters as a source of new atmospheric particles, Nature, 404, 66–69, 2000. 25742

Langridge, J. M., Ball, S. M., Shillings, A. J. L., and Jones, R. L.: A broadband absorption spectromenter using light emitting diodes for ultrasensitive, in situ trace gas detection, Rev.

Sci. Instrum., 79(123), 110–114, 2008. 25752
Leigh, R. J., Corlett, G. K., Friess, U., and Monks, P.: A concurrent multi-axis differential optical absorption spectroscopy system for the measurement of tropospheric nitrogen dioxide, Appl. Optics, 45, 7504–7518, 2006. 25754

Leigh, R. J., Ball, S. M., Whitehead, J., Leblanc, C., Shillings, A. J. L., Mahajan, A. S., Oetjen, H., Dorsey, J. R., Gallagher, M., Jones, R. L., Plane, J. M. C., Potin, P., and McFiggans, G.: Measurements and modelling of molecular iodine emissions, transport and photodestruction in the coastal region around Roscoff, Atmos. Chem. Phys. Discuss., 9, 21165–21198, 2009, http://www.atmos-chem-phys-discuss.net/9/21165/2009/. 25744, 25753

Mahajan, A. S., Oetjen, H., Saiz-Lopez, A., Lee, J. D., McFiggans, G. B., and Plane, J. M. C.: Reactive iodine species in a semi-polluted environment, Geophys. Res. Lett., 36, L16803, doi:10.1029/2009GL038018, 2009. 25740, 25751, 25752, 25753

Mahajan, A. S., Plane, J. M. C., Oetjen, H., Mendes, L., Saunders, R. W., Saiz-Lopez, A., Jones, C. E., Carpenter, L. J., and McFiggans, G. B.: Measurement and modelling of reactive halogen species over the tropical Atlantic Ocean, Atmos. Chem. Phys. Discuss., 9, 24281–24316, 2009, http://www.atmos-chem-phys-discuss.net/9/24281/2009/. 25743

Makela, J. M., Hoffmann, T., Holzke, C., Vakeva, M., Suni, T., Mattila, T., Aalto, P. P., Tapper, U., Kauppinen, E. I., and O'Dowd, C. D.: Biogenic iodine emissions and identification of end-products in coastal ultrafine particles during nucleation bursts, J. Geophys. Res., 107(D19), 8110, 2002. 25742

McFiggans, G., Plane, J. M. C., Allan, B. J., Carpenter, L. J., Coe, H., and O'Dowd, C.: A modeling study of iodine chemistry in the marine boundary layer, J. Geophys. Res., 105, 14371–14385, 2000. 25740, 25746

McFiggans, G., Cox, R. A., Mossinger, J. C., Allan, B. J., and Plane, J. M. C.: Active chlorine release from marine aerosol: roles for reactive iodine andnitrogen species, J. Geophys. Res., 107(D15), 4271, doi:10.1029/2001JD000383, 2002. 25740

McFiggans, G., Coe, H., Burgess, R., Allan, J., Cubison, M., Alfarra, M. R., Saunders, R., Saiz-Lopez, A., Plane, J. M. C., Wevill, D., Carpenter, L., Rickard, A. R., and Monks, P. S.: Direct evidence for coastal iodine particles from Laminaria macroalgae - linkage to emissions of molecular iodine, Atmos. Chem. Phys., 4, 701–713, 2004, http://www.atmos-chem-phys.net/4/701/2004/. 25740, 25742

McFiggans, G. B., Bale, C. S. E., Ball, S., Beames, J. M., Bloss, W. J., Carpenter, L. J., Dorsey, J., Dunk, R., Flynn, M. J., Furneaux, K. L., Gallagher, M. W., Heard, D. E., Hollingsworth, A. M., Hornsby, K., Ingham, T., Jones, C. E., Jones, R. L., Kramer, L. J., Langridge, J. M., Leblanc, C., LeCrane, J.-P., Lee, J. D., Leigh, R. J., Longley, I., Mahajan, A. S., Monks, P. S., Oetjen, H., Orr-Ewing, A. J., Plane, J. M. C., Potin, P., Shillings, A. J. L., Thomas, F., von Glasow, R., Wada, R., Whalley, L. K., and Whitehead J. D.: Iodine-mediated coastal particle formation: an overview of the Reactive Halogens in the Marine Boundary Layer (RHaMBLe) Roscoff coastal study, Atmos. Chem. Phys. Discuss., in preparation, 2009. 25741, 25743, 25744, 25749, 25751, 25754

Mossinger, J. C., Shallcross, D. E., and Cox, R.: UV-VIS absorption cross-sections and atmospheric lifetimes of CH_2Br_2, CH_2I_2, and CH_2BrI, J. Chem. Soc. Faraday T., 94, 1391–1396, 1998. 25777

O'Dowd, C., McFiggans, G., Creasey, D. J., Pirjola, L., Hoell, C., Smith, M. H., Allan, B. J., Plane, J. M. C., Heard, D. E., Lee, J. D., Pilling, M. J., and Kulmala, M.: On the photochemical production of new particles in the coastal boundary layer, Geophys. Res. Lett., 26, 1707–1710, 1999. 25742

O'Dowd, C. D., Jimenez, J. L., Bahreini, R., Flagan, R. C., Seinfeld, J. H., Hameri, K., Pirjola, L., Kulmala, M., and Jennings, S. G.: Marine aerosol formation from biogenic emissions, Nature, 417, 632–636, 2002. 25740, 25742

Orlando, J. J. and Tyndall, G. S.: Rate Coefficients for the Thermal Decomposition of $BrONO_2$ and the Heat of Formation of $BrONO_2$, J. Phys. Chem., 100, 19398–19405, 1996. 25773, 25775

Palmer, C. J., Anders, T. L., Carpenter, L. J., Kupper, F. C., and McFiggans, G. B.: Iodine and Halocarbon Response of Laminaria digitata to Oxidative Stress and Links to Atmospheric New Particle Production, Environ. Chem., 2, 282–290, 2005. 25742

Passchier, A., Christian, J., and Gregory, N.: The ultraviolet-visible absorption spectrum of bromine between room temperature and 440 degrees C, J. Phys. Chem., 71, 937–942, 1967. 25777

Pechtl, S., Lovejoy, E. R., Burkholder, J. B., and von Glasow, R.: Modeling the possible role of iodine oxides in atmospheric new particle formation, Atmos. Chem. Phys., 6, 505–523, 2006, http://www.atmos-chem-phys.net/6/505/2006/. 25741

Pechtl, S., Schmitz, G., and von Glasow, R.: Modelling iodide - iodate speciation in atmospheric aerosol: Contributions of inorganic and organic iodine chemistry, Atmos. Chem. Phys., 7, 1381–1393, 2007, http://www.atmos-chem-phys.net/7/1381/2007/. 25742, 25746

Peters, C., Pechtl, S., Stutz, J., Hebestreit, K., Hönninger, G., Heumann, K. G., Schwarz, A., Winterlik, J., and Platt, U.: Reactive and organic halogen species in three different European coastal environments, Atmos. Chem. Phys., 5, 3357–3375, 2005, http://www.atmos-chem-phys.net/5/3357/2005/. 25740, 25747, 25748

Pirjola, L., O'Dowd, C. D., Yoon, Y. J., and Sellegri, K.: Modelling Iodine Particle Formation and Growth from Seaweed in a Chamber, Environ. Chem., 2, 271–281, 2005. 25742

Plane, J., Joseph, D., Allan, B., Ashworth, S., and Francisco, J.: An Experimental and Theoretical Study of the Reactions OIO+NO and OIO+OH, J. Phys. Chem. A, 110, 93–100, 2006. 25774

Platt, U. and Hönninger, G.: The role of halogen species in the troposphere, Chemosphere, 51, 325–338, 2003. 25740

Ravishankara, A. R.: Heterogeneous and multiphase chemistry in the troposphere, Science, 276, 1058–1065, 1997. 25746

Read, K. A., Mahajan, A. S., Carpenter, L. J., Evans, M. J., Bruno, V. E. F., Heard, D. E., Hopkins, J. R., Lee, J. D., Moller, S. J., Lewis, A. C., Mendes, L., McQuaid, J. B., Oetjen, H., Saiz-Lopez, A., Pilling, M. J., and Plane, J. M. C.: Extensive halogen-mediated ozone destruction over the tropical Atlantic Ocean, Nature, 453, 1232–1235, 26 June, 2008. 25740, 25759

Roehl, C. M., Burkholder, J. B., Moortgat, G. K., Ravishankara, A. R., and Crutzen, P. J.: Temperature dependence of UV absorption cross sections and atmospheric implications of several alkyl iodides, J. Geophys. Res.-Atmos., 102, 12819–12829, 1997. 25777

Saiz-Lopez, A. and Plane, J. M. C.: Novel iodine chemistry in the marine boundary layer, Geophys. Res. Letts., 31, 19215–19218, 2004. 25740

Saiz-Lopez, A., Saunders, R. W., Joseph, D. M., Ashworth, S. H., and Plane, J. M. C.: Absolute absorption cross-section and photolysis rate of I_2, Atmos. Chem. Phys., 4, 1443–1450, 2004, http://www.atmos-chem-phys.net/4/1443/2004/. 25748, 25777

Saiz-Lopez, A., Plane, J. M. C., McFiggans, G., Williams, P. I., Ball, S. M., Bitter, M., Jones, R. L., Hongwei, C., and Hoffmann, T.: Modelling molecular iodine emissions in a coastal marine environment: the link to new particle formation, Atmos. Chem. Phys., 6, 883–895, 2006, http://www.atmos-chem-phys.net/6/883/2006/. 25741, 25742, 25743

Saiz-Lopez, A., Shillito, J. A., Coe, H., and Plane, J. M. C.: Measurements and modelling of I_2, IO, OIO, BrO and NO_3 in the mid-latitude marine boundary layer, Atmos. Chem. Phys., 6, 1513–1528, 2006, http://www.atmos-chem-phys.net/6/1513/2006/. 25747

Saiz-Lopez, A., Plane, J. M. C., Mahajan, A. S., Anderson, P. S., Bauguitte, S. J.-B., Jones, A. E., Roscoe, H. K., Salmon, R. A., Bloss, W. J., Lee, J. D., and Heard, D. E.: On the vertical distribution of boundary layer halogens over coastal Antarctica: implications for O_3, HO_x, NO_x and the Hg lifetime, Atmos. Chem. Phys., 8, 887–900, 2008, http://www.atmos-chem-phys.net/8/887/2008/. 25773, 25774, 25775, 25776, 25778

Sander, S. P., Friedl, R. R., Golden, D. M., Kurylo, M. J., Moortgat, C. K., Keller-Rudek, H., Wine, P. H., Ravishankara, A. R., Kolb, C. E., Molina, M. J., Finlayson-Pitts, B. J., Huie, R. E., and Orkin, V. L.: Chemical kinetics and photochemical data for use in atmospheric Studies, Evaluation number 15, NASA Jet Propulsion Laboratory, Publication 062, 2006. 25773, 25774, 25775, 25776, 25777

Saunders, R. W. and Plane, J. M. C.: Formation Pathways and Composition of Iodine Oxide Ultra-Fine Particles, Environ. Chem., 2, 299–303, 2005. 25742, 25774

Saunders, S. M., Jenkin, M. E., Derwent, R. G., and Pilling, M. J.: Protocol for the development of the Master Chemical Mechanism, MCM v3 (Part A): tropospheric degradation of non-aromatic volatile organic compounds, Atmos. Chem. Phys., 3, 161–180, 2003, http://www.atmos-chem-phys.net/3/161/2003/. 25746

Sellegri, K., Yoon, Y. J., Jennings, S. G., O'Dowd, C. D., Pirjola, L., Cautenet, S., Chen, H., and Hoffmann, T.: Quantification of Coastal New ultra-fine Particle Formation from In situ and Chamber Measurements during the BIOFLUX campaign, Environ. Chem., 2, 260–270, 2005. 25742

Sommariva, R., Bloss, W. J., Brough, N., Carslaw, N., Flynn, M., Haggerstone, A.-L., Heard, D. E., Hopkins, J. R., Lee, J. D., Lewis, A. C., McFiggans, G., Monks, P. S., Penkett, S. A., Pilling, M. J., Plane, J. M. C., Read, K. A., Saiz-Lopez, A., Rickard, A. R., and Williams, P. I.: OH and HO_2 chemistry during NAMBLEX: roles of oxygenates, halogen oxides and heterogeneous uptake, Atmos. Chem. Phys., 6, 1135–1153, 2006, http://www.atmos-chem-phys.net/6/1135/2006/. 25741

Stutz, J., Hebestreit, K., Alicke, B., and Platt, U.: Chemistry of Halogen Oxides in the troposphere: Comparison of Model Calculations with Recent Field Data, J. Atmos. Chem., 34, 65–85, 1999. 25759

Stutz, J., Pikelnaya, O., Hurlock, S. C., Trick, S., Pechtl, S., and von Glasow, R.: Daytime OIO in the Gulf of Maine, Geophys. Res. Lett., 34, L22816, doi:10.1029/2007GL031332, 2007.

25740, 25741, 25748, 25749, 25752

Vogt, R., Crutzen, P. J., and Sander, R.: A mechanism for halogen release from sea-salt aerosol in the remote marineboundary layer, Nature, 383, 327–330, 1996. 25740

Vogt, R., Sander, R., von Glasow, R., and Crutzen, P. J.: Iodine Chemistry and its Role in Halogen Activation and Ozone Loss in the Marine Boundary Layer: A Model Study, J. Atmos. Chem., 32, 375–395, 1999. 25746

von Glasow, R. and Crutzen, P. J.: Treatise On Geochemistry: 4.02 Tropspheric Halogen Chemistry, Elsevier, iSBN (set): 0-08-043751-6, 2007. 25754

Wada, R., Beames, J. M., and Orr-Ewing, A. J.: Measurement of IO radical concentrations in the marine boundary layer using a cavity ring-down spectrometer, J. Atmos. Chem., 58, 69–87, 2007. 25754

Whalley, L. K., Furneaux, K. L., Gravestock, T., Atkinson, H. M., Bale, C. S. E., Ingham, T., Bloss, W. J., and Heard, D. E.: Detection of Iodine Monoxide Radicals in the Marine Boundary Layer using Laser Induced Fluorescence Spectroscopy, J. Atmos. Chem., 58, 19–39, 2007. 25743, 25744, 25745, 25753

Whalley, L. K., Furneaux, K. L., Goddard, A., Lee, J. D., Mahajan, A., Oetjen, H., Read, K. A., Kaaden, N., Carpenter, L. J., Lewis, A. C., Plane, J. M. C., Saltzman, E. S., Wiedensohler, A., and Heard, D. E.: The chemistry of OH and HO_2 radicals in the boundary layer over the tropical Atlantic Ocean, Atmos. Chem. Phys. Discuss., 9, 15959–16009, 2009, http://www.atmos-chem-phys-discuss.net/9/15959/2009/. 25759

Whitehead, J. D., McFiggans, G. B., Gallagher, M. W., and Flynn, M. J.: Direct linkage between tidally driven coastal ozone deposition fluxes, particle emission fluxes and subsequent CCN formation, Geophys. Res. Lett., 105, L04806, doi:doi:10.1029/2008GL035969, 2009. 25746, 25757, 25758

Table 1. Summary of parameters used by the model to simulate night-time IO observations.

Species	8–9 September	25–25 September
I_2/pptv	50	50
CH_3I/pptv	0.5	0.5
CH_2IBr/pptv	0.02	0.02
DMS/pptv	20	20
NO/ppbv	0.033	0.117
NO_2/ppbv	2.23	2.42
NO_3/pptv	40	40
O_3/ppbv	31.6	19.2

Table 2. Summary of the performance of the IO measurement techniques. Instrument detection limits are an average daytime value for 8 September. Detection limits are quoted as mixing ratios except the CMAX-DOAS measurements, which is a slant column.

Instrument	Detection Limit	Integration Period
LIF	0.4 pptv	150 s
	1.1 pptv	10 s
LP-DOAS	0.6 pptv	60 s
CRDS	12 pptv	30 s
CMAX-DOAS	1.64×10^{13} molecule cm^{-2}	15 min

Table A1. Halogen chemistry reaction scheme – unimolecular reactions.

Unimolecular reactions		
Reaction	Rate coefficient/s^{-1}	Reference
$INO_2 \rightarrow I+NO_2$	$(2.4/0.005)2.07\times10^{15}\exp(-11859/T)$	Saiz-Lopez et al. (2008)
$IONO_2 \rightarrow IO+NO_2$	$2.1\times10^{15}\exp(-13670/T)$	Sander et al. (2006)
$I_2O_2 \rightarrow I+OIO$	10	Kaltsoyannis and Plane (2008)
$I_2O_2 \rightarrow 2IO$	0.045	Kaltsoyannis and Plane (2008)
$I_2O_4 \rightarrow 2OIO$	0.038	Kaltsoyannis and Plane (2008)
$BrNO_3 \rightarrow BrO+NO_2$	$2.8\times10^{13}\exp(-12360/T)$	Orlando and Tyndall (1996)

Table A2. Halogen chemistry reaction scheme – bimolecular reactions. DMS = dimethyl sulphide.

Bimolecular reactions		
Reaction	Rate coefficient/cm^3 molecule^{-1} s^{-1}	Reference
$I_2+OH \rightarrow HOI+I$	1.8×10^{-10}	Sander et al. (2006)
$I_2+O_3 \rightarrow IO+I+O_2$	3.8×10^{-18}	Saiz-Lopez et al. (2008)
$I_2+O_3 \rightarrow OIO+IO$	3.8×10^{-18}	Saiz-Lopez et al. (2008)
$I_2+NO_3 \rightarrow I+IONO_2$	1.5×10^{-12}	Atkinson et al. (2007)
$I+O_3 \rightarrow IO+O_2$	$2.3\times10^{-11}\exp(-870/T)$	Sander et al. (2006)
$I+HO_2 \rightarrow HI+O_2$	$1.5\times10^{-11}\exp(-1090/T)$	Sander et al. (2006)
$I+NO_3 \rightarrow IO+NO_2$	4.5×10^{-10}	Chambers et al. (1992)
$IO+HO_2 \rightarrow HOI+O_2$	$1.4\times10^{-11}\exp(540/T)$	Atkinson et al. (2007)
$IO+NO \rightarrow I+NO_2$	$9.1\times10^{-12}\exp(240/T)$	Sander et al. (2006)
$IO+IO \rightarrow 0.38\ OIO+I$	$5.4\times10^{-11}\exp(180/T)$	Atkinson et al. (2007)
$IO+IO \rightarrow 0.51\ I_2O_2$	$5.4\times10^{-11}\exp(180/T)$	Atkinson et al. (2007)
$IO+IO \rightarrow 0.11\ 2I+O_2$	$5.4\times10^{-11}\exp(180/T)$	Atkinson et al. (2007)
$IO+DMS \rightarrow I+DMSO$	$9.6\times10^{-12}\exp(-1816/T)$	Gravestock et al. (2005)
$IO+OI \rightarrow I_2O_3$	5×10^{-11}	Gomez Martin et al. (2007)
$IO+NO_3 \rightarrow OIO+NO_2$	9×10^{-12}	Dillon et al. (2008)
$OIO+OIO \rightarrow I_2O_4$	1.2×10^{-10}	Gomez Martin et al. (2007)
$OIO+OH \rightarrow HOIO_2$	$2.2\times10^{-10}\exp(243/T)$	Plane et al. (2006)
$OIO+NO \rightarrow O+NO_2$	$1.1\times10^{-12}\exp(542/T)$	Plane et al. (2006)
$I_2O_2+O_3 \rightarrow I_2O_3+O_2$	1×10^{-12}	Saunders and Plane (2005)
$I_2O_3+O_3 \rightarrow I_2O_4+O_2$	1×10^{-12}	Saunders and Plane (2005)
$I_2O_4+O_3 \rightarrow I_2O_5+O_2$	1×10^{-12}	Saunders and Plane (2005)

Title Page
Abstract Introduction
Conclusions References
Tables Figures
◀| |▶
◀ ▶
Back Close
Full Screen / Esc
Printer-friendly Version
Interactive Discussion

Table A2. Continued.

	Bimolecular reactions	
Reaction	Rate coefficient/cm^3 molecule^{-1} s^{-1}	Reference
$HOI+OH \rightarrow IO+H_2O$	2×10^{-13}	Saiz-Lopez et al. (2008)
$HI+OH \rightarrow I+H_2O$	3.0×10^{-11}	Sander et al. (2006)
$Br_2+OH \rightarrow HOBr+Br$	$2.1\times10^{-11}\exp(240/T)$	Sander et al. (2006)
$Br+HO_2 \rightarrow HBr+O_2$	$4.8\times10^{-12}\exp(-310/T)$	Sander et al. (2006)
$Br+O_3 \rightarrow BrO+O_2$	$1.7\times10^{-11}\exp(-800/T)$	Sander et al. (2006)
$Br+HCHO \rightarrow HBr+HCO$	$1.7\times10^{-11}\exp(-800/T)$	Sander et al. (2006)
$Br+CH_3CHO \rightarrow HBr+CH_3CO$	$1.3\times10^{-11}\exp(-360/T)$	Atkinson et al. (2002)
$BrO+O \rightarrow Br+O_2$	$1.9\times10^{-11}\exp(230/T)$	Sander et al. (2006)
$BrO+OH \rightarrow HO_2+Br$	$1.7\times10^{-11}\exp(250/T)$	Sander et al. (2006)
$BrO+HO_2 \rightarrow HOBr+O_2$	$4.5\times10^{-12}\exp(460/T)$	Sander et al. (2006)
$BrO+NO \rightarrow NO_2+Br$	$8.8\times10^{-12}\exp(260/T)$	Sander et al. (2006)
$BrO+BrO \rightarrow Br+Br+O_2$	$2.4\times10^{-12}\exp(40/T)$	Sander et al. (2006)
$BrO+BrO \rightarrow Br_2+O_2$	$2.8\times10^{-14}\exp(860/T)$	Sander et al. (2006)
$BrO+IO \rightarrow 0.3(Br+I+O_2)+0.7\ (Br+OIO)$	$2.5\times10^{-11}\exp(260/T)$	Sander et al. (2006)
$BrO+I \rightarrow IO+Br$	1.2×10^{-11}	Sander et al. (2006)
$BrO+DMS \rightarrow Br+DMSO$	$1.5\times10^{-14}\exp(850/T)$	Sander et al. (2006)
$HOBr+O \rightarrow OH+BrO$	$1.2\times10^{-10}\exp(-430/T)$	Sander et al. (2006)
$HBr+OH \rightarrow H_2O+Br$	$5.5\times10^{-12}\exp(200/T)$	Sander et al. (2006)
$BrNO_3+I \rightarrow IBr+NO_3$	2.0×10^{-10}	estimated from the rate coefficient of $BrNO_3$+ Br
$BrNO_3+Br \rightarrow Br_2+NO_3$	4.9×10^{-11}	Orlando and Tyndall (1996)
$BrNO_3+NO \rightarrow BrNO+NO_3$	3×10^{-19}	Orlando and Tyndall (1996)
$BrNO_3+BrNO \rightarrow Br_2+2NO_2$	1×10^{-16}	Orlando and Tyndall (1996)

Table A3. Halogen chemistry reaction scheme – termolecular reactions.

Termolecular reactions

$$k_r = k_0/k_\infty$$

$$F = 10^{\log F_c/(1+[\log k_r]^2)}$$

$$k = ([k_0 k_\infty]/[k_0 + k_\infty])F$$

Reaction	Rate coefficient (k) k_0/cm^6 molecule^{-2} s^{-1} k_∞/cm^3 molecule^{-1} s^{-1}	Reference
$I+NO_2+M \rightarrow INO_2+M$	$k_0=(3\times10^{-31}M)/(T/300)$ $k_\infty=6.6\times10^{-11}$ $F_c=\exp(-T/650)+\exp(-2600/T)$	Sander et al. (2006), F_c – Saiz-Lopez et al. (2008)
$I+NO+M \rightarrow INO+M$	$k_0=(1.8\times10^{-32}M)/(T/300)$ $k_\infty=1.7\times10^{-11}$ $F_c=0.6$	Atkinson et al. (2007)
$IO+NO_2+M \rightarrow IONO_2+M$	$k_0=(7.7\times10^{-31}M)/(T/300)^5$ $k_\infty=1.6\times10^{-11}$ $F_c=0.4$	Atkinson et al. (2007)
$Br+NO_2+M \rightarrow BrNO_2+M$	$k_0=(4.2\times10^{-31}M)/(T/300)^{2.4}$ $k_\infty=2.7\times10^{-11}$ $F_c=0.55$	Atkinson et al. (2007)
$BrO+NO_2+M \rightarrow BrNO_3+M$	$k_0=(5.2\times10^{-31}M)/(T/300)^{3.1}$ $k_\infty=1.8\times10^{-11}$ $F_c=0.6$	Atkinson et al. (2007)

Title Page
Abstract Introduction
Conclusions References
Tables Figures
◀▎ ▶▎
◀ ▶
Back Close
Full Screen / Esc
Printer-friendly Version
Interactive Discussion

Table A4. Halogen chemistry reaction scheme – photochemical reactions. Citation refers to recommended absorption cross section and quantum yield.

Halogen Photolysis	
Photochemical reactions	Reference
$I_2 \rightarrow 2I$	Saiz-Lopez et al. (2004)
$IO \rightarrow I+O$	Sander et al. (2006)
$OIO \rightarrow I+O_2$	Gomez Martin et al. (2009)
$HOI \rightarrow I+OH$	Sander et al. (2006)
$INO_2 \rightarrow 0.5(I+NO_2)/0.5(IO+NO)$	Sander et al. (2006)
$IONO_2 \rightarrow I+NO_3$	Joseph et al. (2007)
$CH_3I \rightarrow CH_3+I$	Atkinson et al. (2004)
$CH_2I_2 \rightarrow CH_2+2I$	Roehl et al. (1997)
$CH_2IBr \rightarrow CH_2+I+Br$	Mossinger et al. (1998)
$INO \rightarrow I+NO$	Sander et al. (2006)
$Br_2 \rightarrow 2Br$	Passchier et al. (1967)
$BrO \rightarrow Br+O$	Atkinson et al. (2007)
$HOBr \rightarrow Br+OH$	Atkinson et al. (2007)
$BrNO_2 \rightarrow Br+NO_2$	Atkinson et al. (2007)
$BrNO_3 \rightarrow Br+NO_3$	Atkinson et al. (2007)
$IBr \rightarrow I+Br$	Atkinson et al. (2007)

Table A5. Halogen chemistry reaction scheme – loss to aerosol.

Loss to aerosol		
Species	Uptake coefficient	Reference
IO	0.02	Saiz-Lopez et al. (2008)
OIO	1	Saiz-Lopez et al. (2008)
HI	0.02	Saiz-Lopez et al. (2008)
HOI	0.02	Saiz-Lopez et al. (2008)
INO_2	0.02	Saiz-Lopez et al. (2008)
$IONO_2$	0.02	Saiz-Lopez et al. (2008)
I_2O_5	0.02	Saiz-Lopez et al. (2008)
N_2O_5	0.03	Saiz-Lopez et al. (2008)
NO_3	0.003	Saiz-Lopez et al. (2008)
OH	$1.2\times10^{-5}\exp(1750/T)$	Saiz-Lopez et al. (2008)
HO_2	$1.4\times10^{-8}\exp(3780/T)$	Saiz-Lopez et al. (2008)
CH_3O_2	0.004	Saiz-Lopez et al. (2008)
HNO_3	0.014	Saiz-Lopez et al. (2008)
NO_2	0.0004	Jacob (2000)
HOBr	0.02	Saiz-Lopez et al. (2008)
HBr	0.02	Saiz-Lopez et al. (2008)
$BrNO_3$	0.02	Saiz-Lopez et al. (2008)

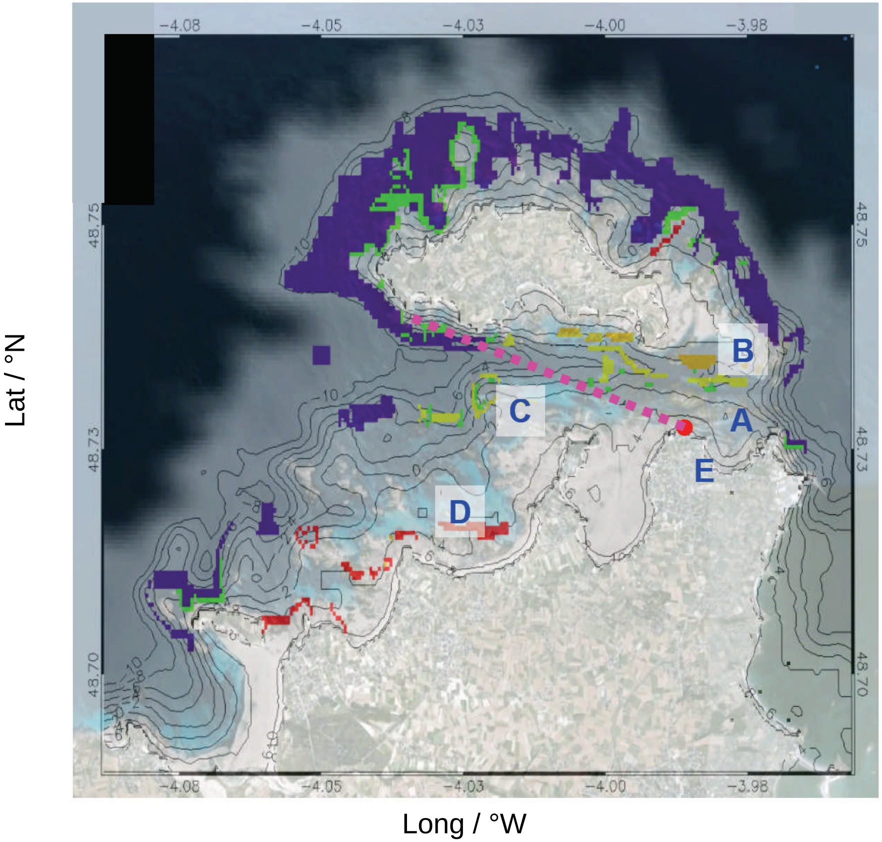

Fig. 1. Map of macroalgae for the Roscoff area. Known emitters of iodine species are *Laminaria digitata* (green), *Laminaria hyperborea* (purple), *Laminaria ochroleuca* (yellow), *Laminaria saccharina* (orange) and *Ascophyllum/Fucus* (red). The red dot marks the location of the LIF instrument. The dashed pink line represents the LP-DOAS light path. Letters refer to macroalgae areas referred to in the text.

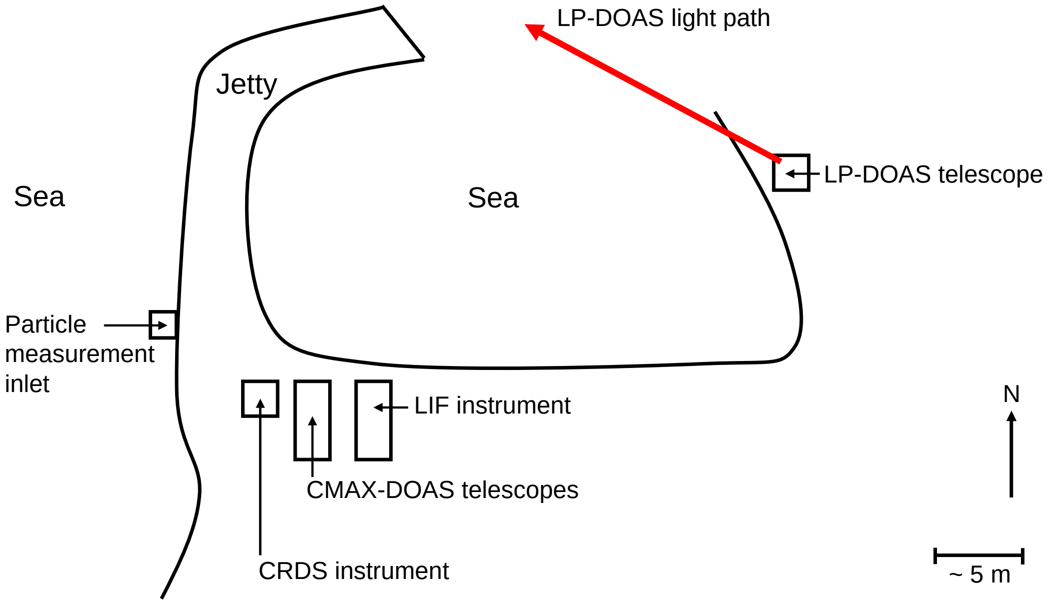

Fig. 2. A schematic of the Roscoff measurement site at high tide. Highlighted instrumentation includes LIF, LP-DOAS, Concurrent Multi Axis DOAS (CMAS-DOAS), Cavity Ringdown Spectroscopy (CRDS) and particle number and size-distribution measurements.

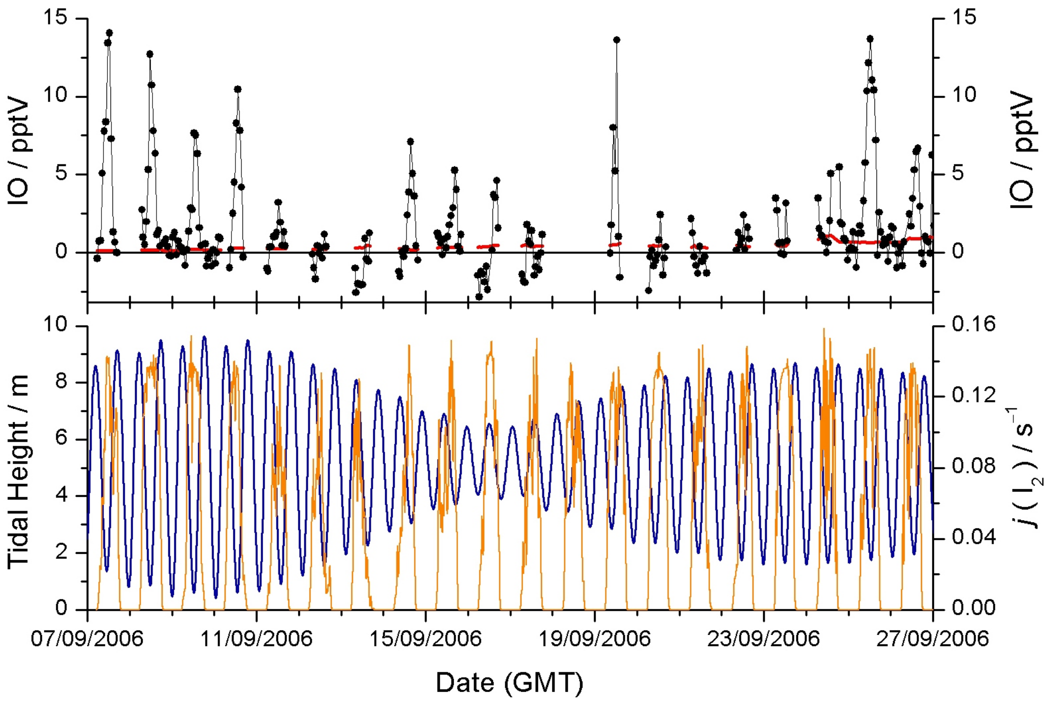

Fig. 3. Time series of IO measurements (23% 1 σ uncertainty, 60 min average, black circles) for the duration of the campaign. Also shown is the IO detection limit (red line), tidal height (blue line) and $j(I_2)$ (ten minute average, orange line).

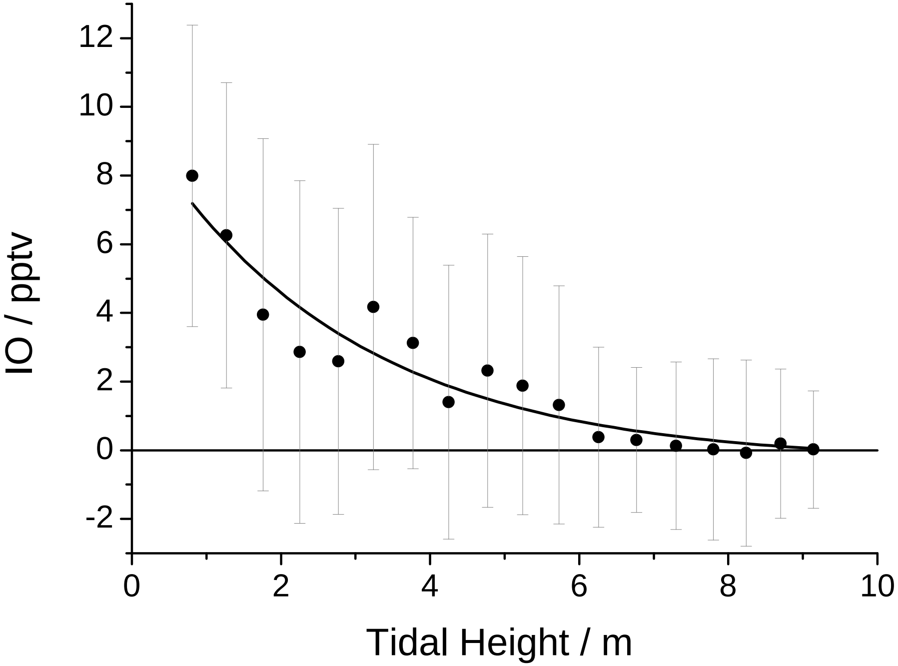

Fig. 4. The relationship between daytime IO and tidal height for the whole campaign (data binned according to 0.5 m width bins of tidal height), using 150 s averaged IO measurements. Error bars represent ±1 σ standard deviation for all binned data. For each tidal height there is a range of $j(I_2)$ depending on the time of day, and other parameters that influence IO, such as NO_x and meteorology. The solid line is an exponential decay fitted to the data, as given in the text by Eq. 2.

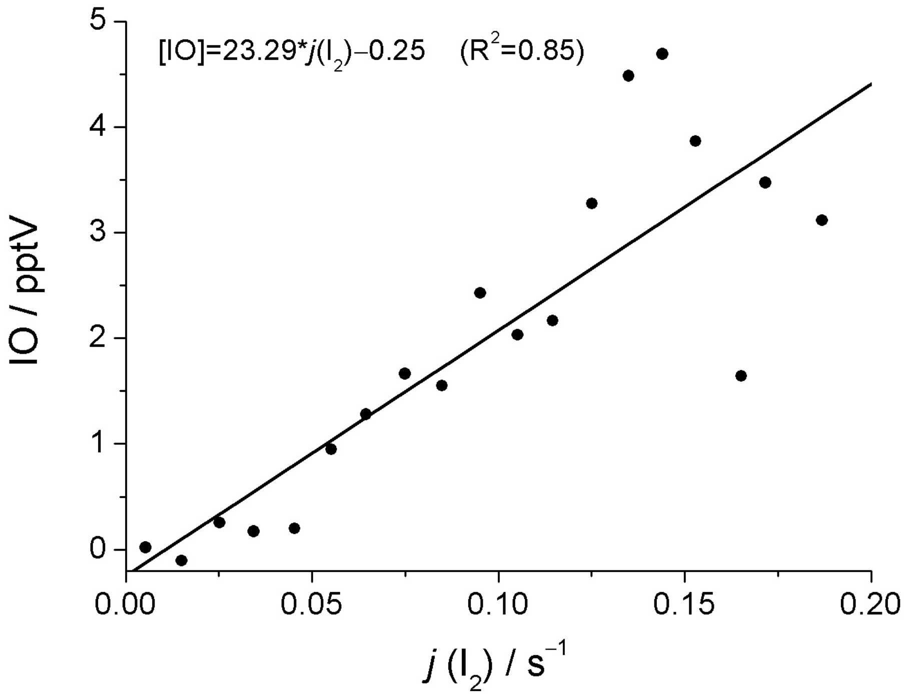

Fig. 5. Correlation plot displaying the relationship of IO with $j(I_2)$ for daytime IO measurements (150 s average) throughout the whole measurement campaign. The data have been binned according to 0.01 s^{-1} sized bins.

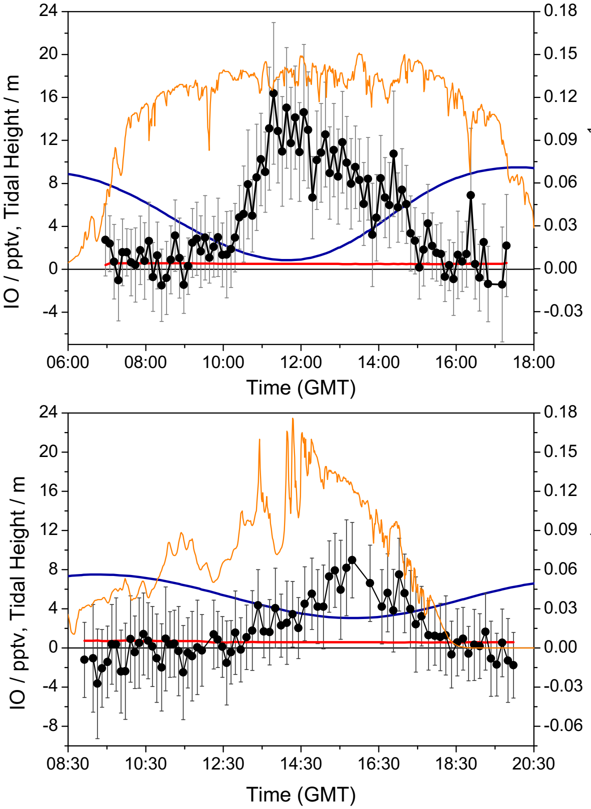

Fig. 6. Daytime IO profiles on 8th September (top) and 14 September (bottom). The black dots represent IO (150 s integration period, error bars represent the 23% 1 σ calibration error combined with the 1% error from the laser power normalisation and the 1 σ precision of the normalised signal), the red line represents the limit of detection (0.8 pptv for 150 s integration period), the orange line represents $j(I_2)$ and the blue line represents tidal height. A clear dependence of IO on tidal height is displayed as IO peaked at the tidal minimum. The bottom panel shows that IO peaked at the tidal minimum rather than peak $j(I_2)$. The variability of IO in the morning and evening around zero is within one standard deviation of the background signal.

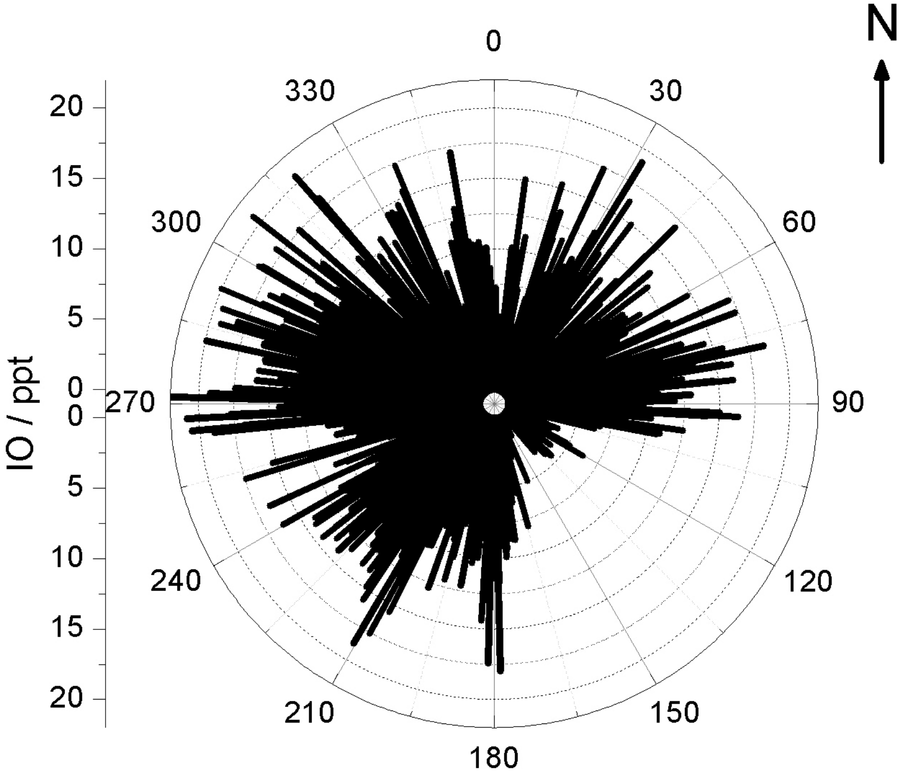

Fig. 7. A wind rose of IO concentrations to demonstrate the dependence of IO concentrations on wind direction (150 s averaged data for the entire campaign). A wind direction of 90 to 180 degrees corresponds to a prevailing wind from the town.

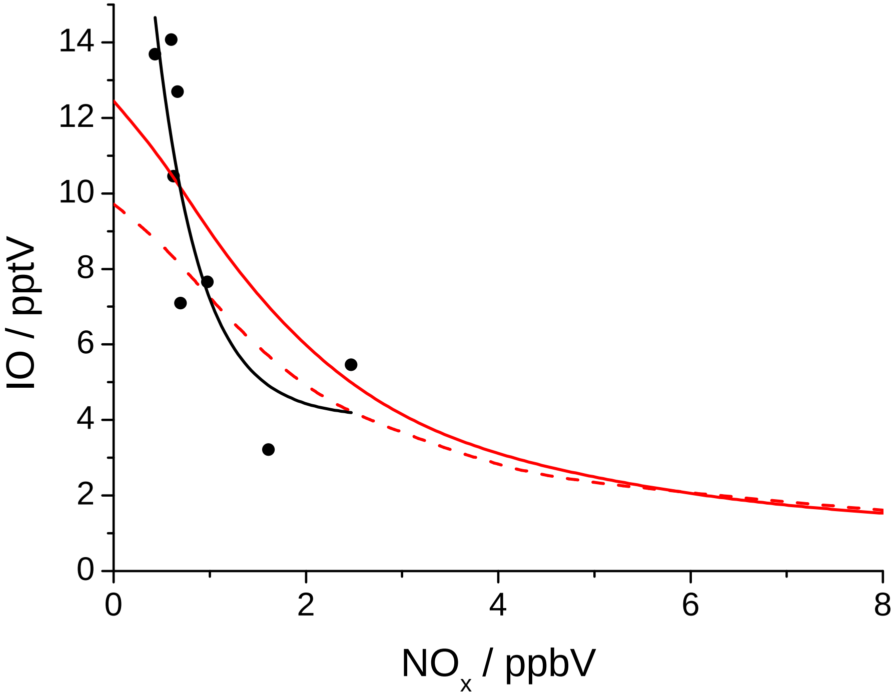

Fig. 8. The dependence of measured IO on NO$_x$ at peak [IO] (black circles). The graph shows how the measured peak [IO] (60 min average) varies with [NO$_x$] (60 min average, at the period of peak IO (30 min either side of peak IO)) for 8 days of the campaign when there was a clear IO diurnal (exponential decay fit, black line, [IO]=4.06+26.6: exp$^{(-[\mathrm{NO_x}]/0.50)}$, R^2=0.77). Model results show a similar IO dependence on NO$_x$, [IO] at 50 s after t=0 s (solid red line) and [IO] at 60 s after t=0 s (dashed red line). Initialised with 100 pptv I_2. Exponential decay fits: [IO]=1.00+11.8: exp$^{(-[\mathrm{NO_x}]/2.40)}$, R^2=0.997 (t=50 s, solid red line), [IO]=0.98+9.02: exp$^{(-[\mathrm{NO_x}]/2.49)}$, R^2=0.996 (t=60 s, dashed red line).

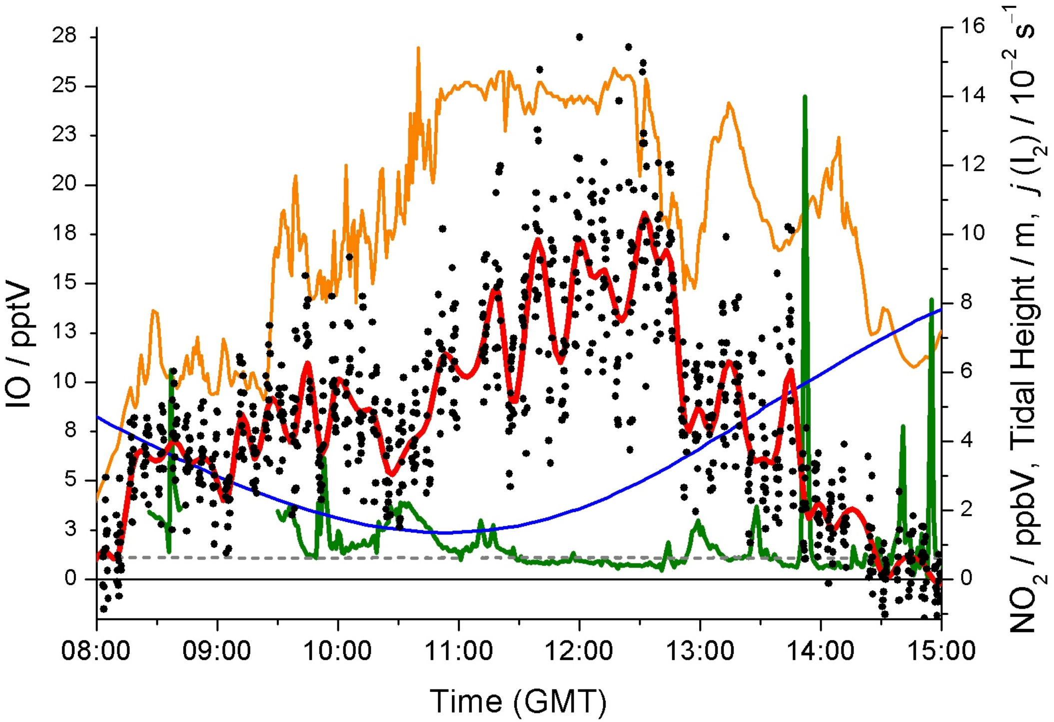

Fig. 9. The IO profile on 7 September. An NO_2 spike (green line) around 10:30 corresponds to a significant decrease in IO concentrations (black circles =10 s integration period, red line =150 s integration period). Also shown is the LIF detection limit (10 s integration period, dashed grey line), tidal height (blue line) and $j(I_2)$ (orange line).

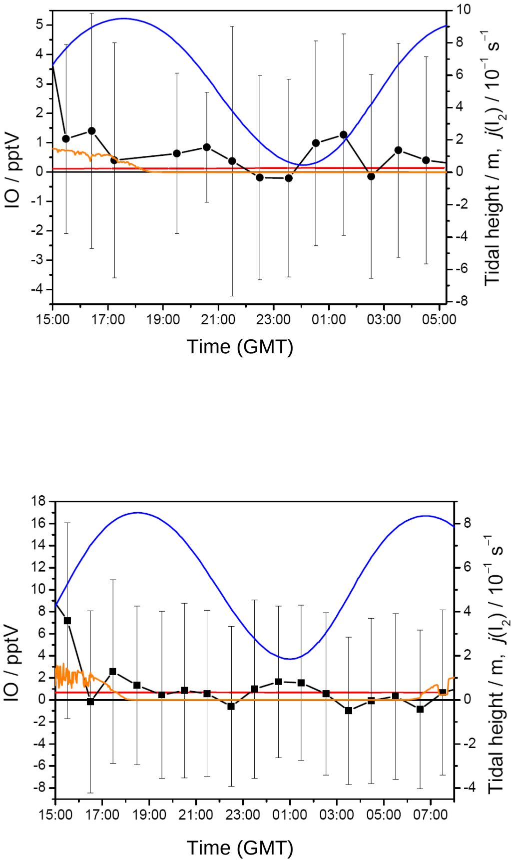

Fig. 10. Night-time measurement of IO on the nights of 8 September (top) and 25 September (bottom). The filled circles (top) and filled squares (bottom) represent IO (60 min average, black line represents 60 min running average, error bars represent the 23% 1 σ calibration error combined with the 1% error from the normalisation and the 1 σ precision of the normalised signal), the red line represents the 60 min limit of detection, the orange line represents $j(I_2)$ and the blue line represents tidal height.

Title Page
Abstract | Introduction
Conclusions | References
Tables | Figures
◀| | |▶
◀ | ▶
Back | Close
Full Screen / Esc

Printer-friendly Version
Interactive Discussion

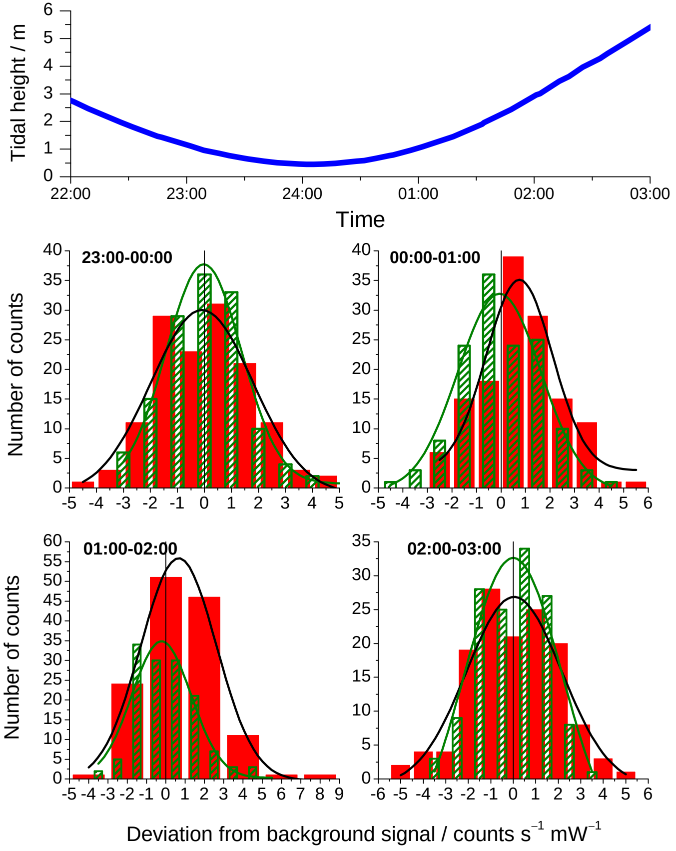

Fig. 11. Analysis of the Gaussian distribution of the LIF signal (middle and bottom panel) on 8–9 September. The red columns represent the distribution of the online deviation from the background (corresponding Gaussian distribution fit is given by a black line) and the hatched green columns represent the distribution of the offline deviation from the mean of the background (corresponding Gaussian distribution fit is given by a green line). The signal is positive between 00:00–02:00, which is just after the tidal minimum (top panel, blue line). The offline Gaussian fit is centred close to zero in all cases.

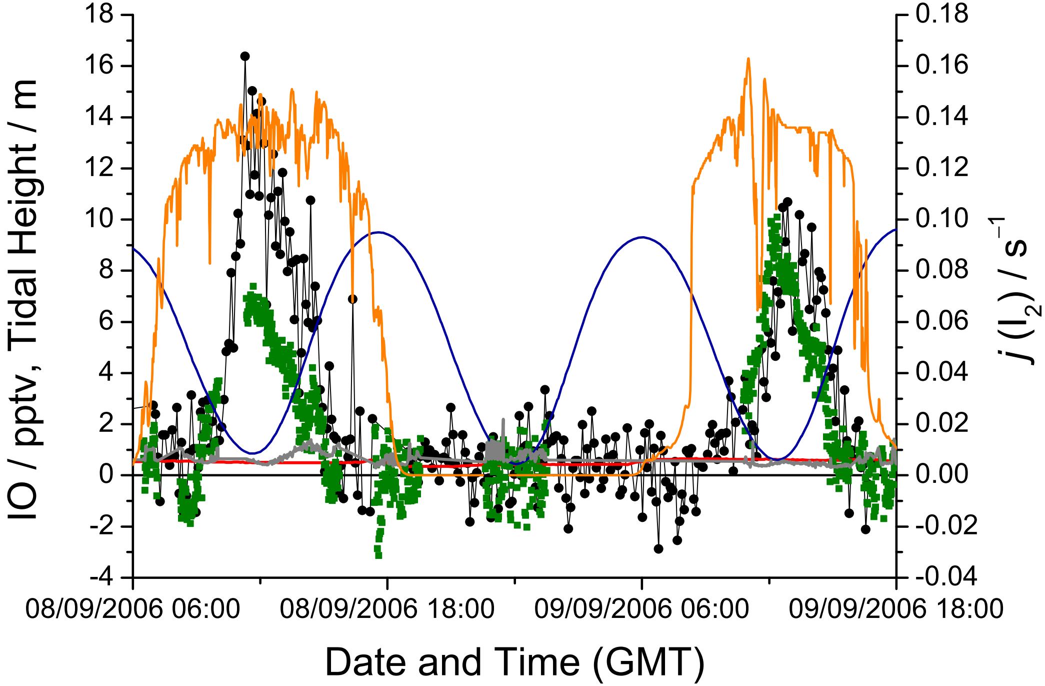

Fig. 12. Time series of 150 s integration period LIF IO measurements (black circles) and 1 min LP-DOAS IO measurements (green squares) from 8 to 9 September. Also shown is the LIF detection limit (red line), LP-DOAS detection limit (grey line), tidal height (blue line) and $j(I_2)$ (orange line).

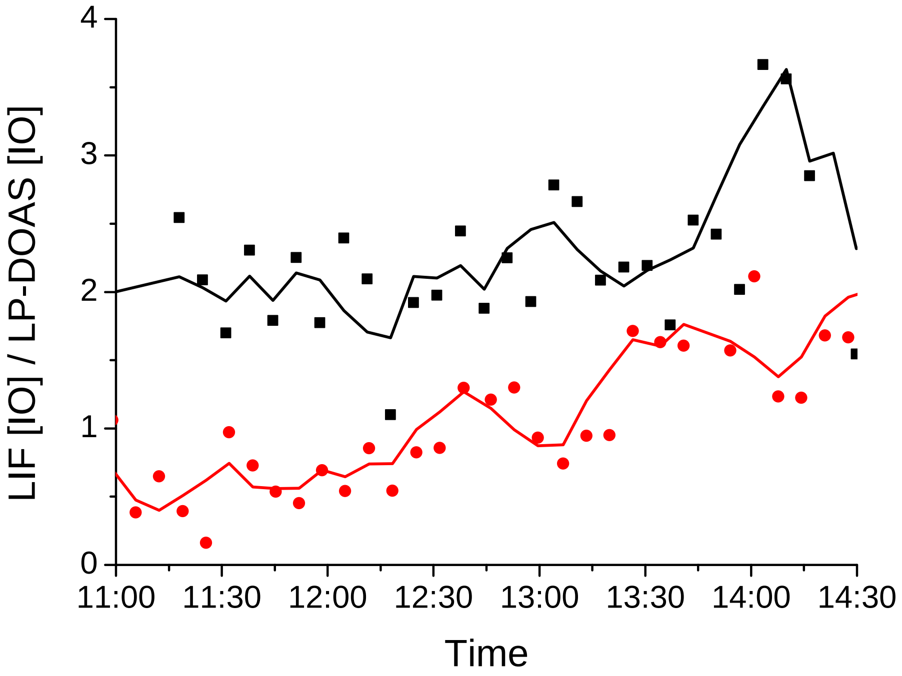

Fig. 13. The ratio of LIF to LP-DOAS [IO] measurements on 8 September (black squares) and 9 September (red circles), with the corresponding 15 min running average (solid line). Low tide was at 11:42 on 8 September and 12:24 on 9 September.

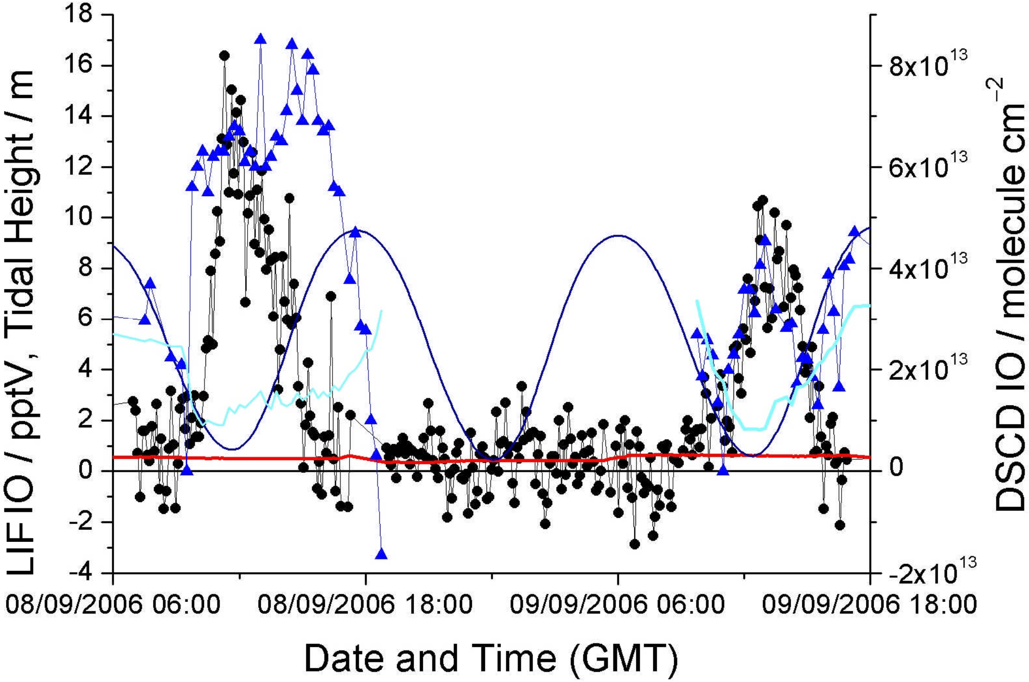

Fig. 14. Time series of 150 s integration period LIF IO mixing ratio measurements (pptv; black circles) and 15 min CMAX-DOAS Differential Slant Column Density (DSCD) IO measurements (molecule cm^{-2}, blue triangles, 5° N-facing telescope) from 8 September to 9 September. Also shown is the LIF detection limit (red line), CMAX-DOAS detection limit (light blue line) and tidal height (blue line).

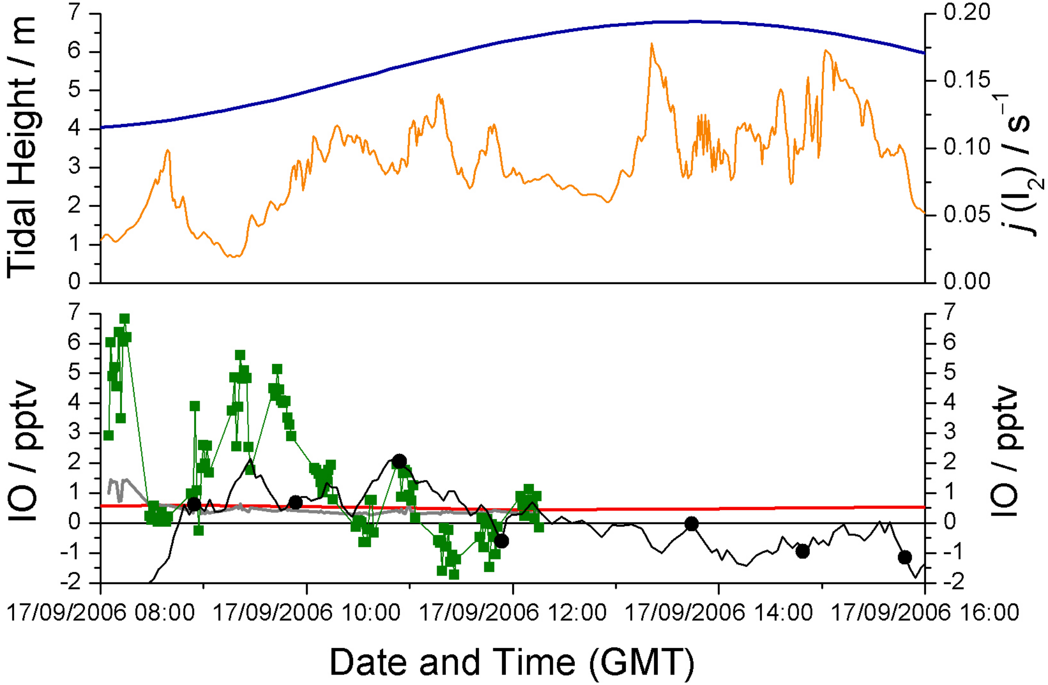

Fig. 15. Top: Tidal height (blue line) and $j(I_2)$ (orange line). Bottom: Time series of 1000 s integration period LIF IO measurements (black circles) and 1 min LP-DOAS IO measurements (green squares) on 17 September. Also shown is the LIF detection limit (red line) and LP-DOAS detection limit (grey line).

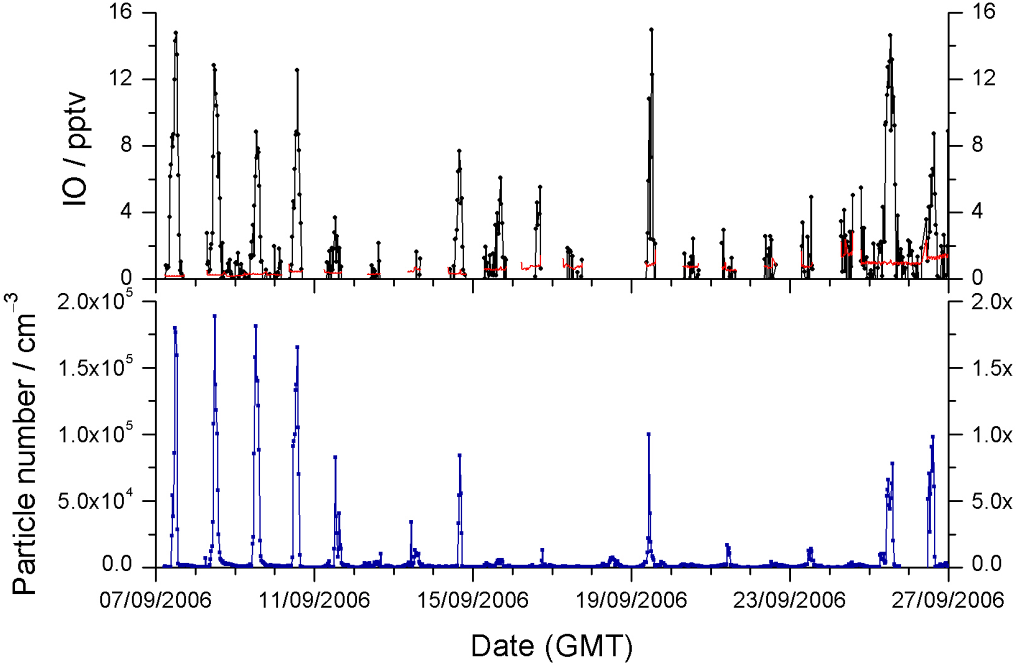

Fig. 16. Time series of IO and particle measurements at Roscoff throughout the campaign. The top panel shows 30 min averaged IO concentrations (black line) with the corresponding 30 min detection limit (red line). No IO measurements were made on 18 September. The bottom panel shows 30 min averaged particle number counts for 2.5 nm<d<10 nm (blue line).

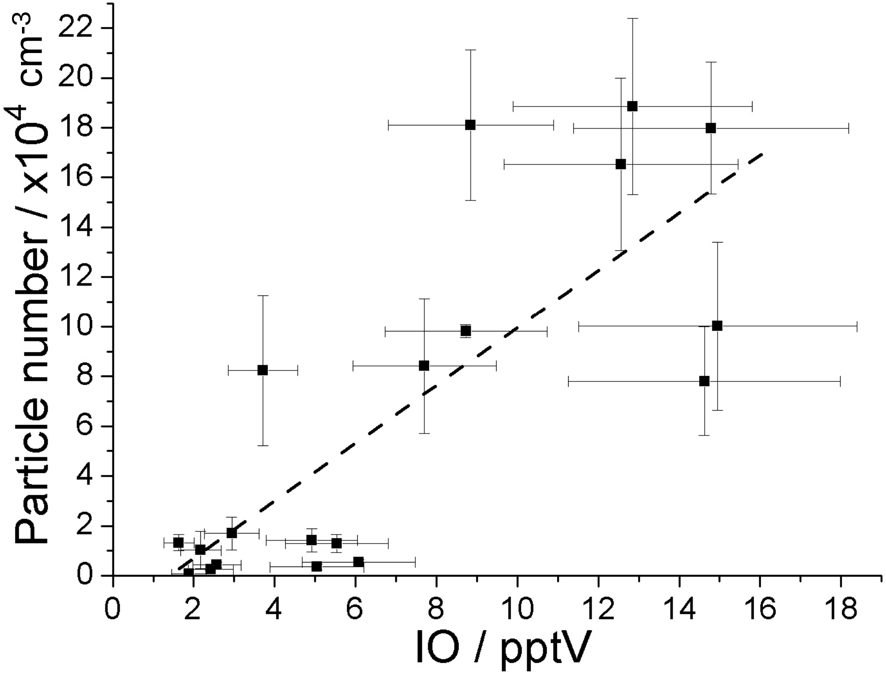

Fig. 17. Correlation plot of peak particle counts (30 min average, 2.5 nm <d<10 nm) against peak IO mixing ratio (30 min average), with 1 σ error, from 7 September to 17 September. The dotted line shows the linear fit (Particle number($\times 10^4$ cm^{-3}=1.2×[IO](pptv)−1.6, R^2=0.8).

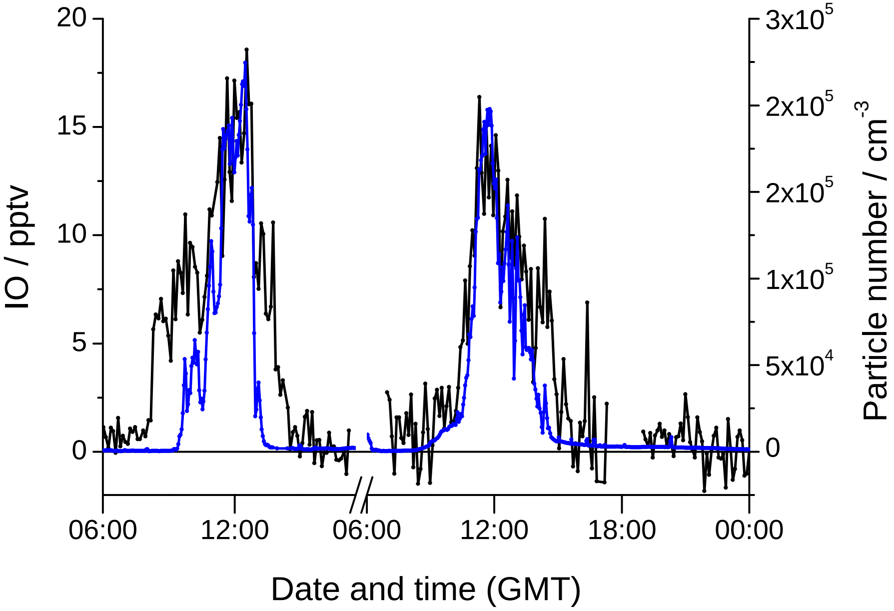

Fig. 18. [IO] (black) and particle number (2.5 nm<d<10 nm, blue) on 7 September and 8 September. IO displays a broader profile than particle number on the 7 September. This is not observed to the same extent on the 8 September, see text for further details.

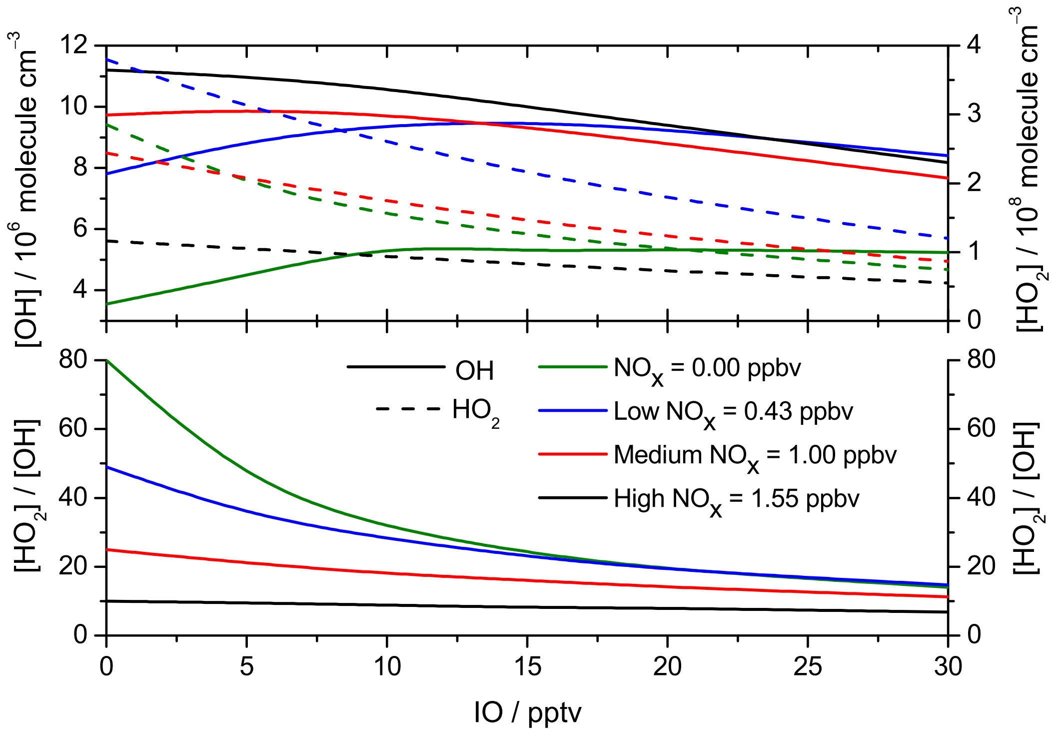

Fig. 19. The effect of IO on OH and HO_2 concentrations and the HO_2/OH ratio at noon at different fixed NO_x concentrations (low NO_x scenario, NO_x=0.43 ppbv, medium NO_x scenario, NO_x=1 ppbv, high NO_x scenario, NO_x=1.55 ppbv). The plot shows how HO_x concentrations vary with increasing IO. The solid line represents [OH] and the dashed line represents [HO_2]. The bottom plot represents the HO_2/OH ratio.